DEPARTMENT OF INFORMATICS

TECHNISCHE UNIVERSITÄT MÜNCHEN

Master's Thesis in Informatics

Investigating dense body surface electrode data for non-invasive detection of intracardiac arrhythmia drivers

Lukas Tenbrink

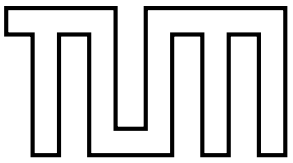

DEPARTMENT OF INFORMATICS

TECHNISCHE UNIVERSITÄT MÜNCHEN

Master's Thesis in Informatics

Investigating dense body surface electrode data for non-invasive detection of intracardiac arrhythmia drivers

Untersuchung dichter Körperoberflächen-Elektroden-Daten für non-invasive Detektion von Herzrhythmusstörungs-Treibern

Author:	Lukas Tenbrink
Supervisor:	Prof. Dr. Daniel Cremers
Advisor:	Dr. Philip Häusser
Submission Date:	15.5.2021

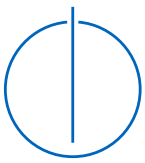

I confirm that this master's thesis in informatics is my own work and I have documented all sources and material used.

Munich, 15.5.2021 Lukas Tenbrink

Acknowledgments

This thesis is the result of long hours of work, close collaboration with and support by many parties. In addition, many methods are presented that build on top of years of previous research. It would not have been possible to complete this alone.

First and foremost, I'd like to thank my advisors, Philip and Peter, for their endless valuable insights and advice. A lot of knowledge about electrographic flow originates from them, and none of this research would have been possible without it. I'd also like to thank Prof. Cremers for facilitating this thesis.

Data from dense body surface electrode configurations is not easy to come by. I'd like to thank the folks from Klinikum der Uni Müenchen for our excellent collaboration and their tireless efforts in gathering data for the prospective dataset. It has been of great use in formulating hypotheses and finally evaluating them in this thesis. An additional thanks goes out to Ajax Health, who kindly provided me with the second dataset. Sourcing from two datasets for optimization and analysis was of great help.

I'd also like to thank my colleagues at Ablacon and AtriomX for providing frameworks and being excellent discussion partners for technical questions.

Finally, I'd like to thank my proof readers for their comments and advice. I truly appreciate the patience!

Abstract

Atrial Fibrillation is the most common arrhythmic disorder of the heart. If left untreated, it can lead to stroke, hospitalization, and death. Effective treatment requires lengthy and costly interventions, yet about half of the patients experience a recurrence in less than a year if the gold standard procedure, pulmonary vein isolation, is performed. A subset of recurrent patients require personalized treatment, which currently can only be provided in specialized centers.

Currently, no meaningful stratification of patients can be performed prior to intervention. Previous studies have often focused on clinical history, single-lead electrocardiograms, or computed tomography-based technologies.

I hypothesized that a novel approach from intracardiac atrial fibrillation mapping, electrographic flow, may be suitable for this task. In this thesis, I present an algorithm capable of deriving knowledge about intracardiac activity from electrodes placed on a patient's torso. I test my hypothesis by examining several modalities. First, the discriminability between individual patients. Second, the discriminability between healthy patients and patients with atrial fibrillation. Third, the predictive power of electrographic flow for spontaneous termination during ablation and long-term recurrence of atrial fibrillation.

The results show that the presented methods perform well in all tasks, with an exception of long-term recurrence prediction. Here the results are inconclusive and a larger-scale study may be needed. I conclude that electrographic flow is a suitable method to map atrial fibrillation on the body surface. Hereby, this work can hopefully contribute to a cost-effective assessment and meaningful stratification of atrial fibrillation patients before ablation.

Contents

1 Introduction

Atrial Fibrillation (AFib) is the most common arrhythmic disorder of the heart, occurring in about 1.5% to 2% of the general population [Cam+12] and in nearly 10% of those over 80 years of age [Kan+98]. It is strongly associated with adverse clinical effects such as stroke, hospitalization and death [Ste+01; Fri+03; WMC03]. AFib stands in contrast to the healthy rhythm of the heart, Sinus Rhythm (SR), and other arrhythmic disorders like atrial flutter.

During AFib, the heart beats irregularly and faster than usual (tachycardia), while the atria are in a constant state of activity. The Sinoatrial (SA) node, which normally regulates the heart rate, is suppressed. AFib patients are often classified as either paroxysmal or persistent. For a classification of paroxysmal AFib, the patient must experience AFib only in short, intermittent intervals (termination in < 7 days [Cal+17]). In contrast, patients with persistent AFib experience AFib most of the time. AFib is a progressive disease: over time, paroxysmal AF worsens to persistent AF [Pad+17] if left untreated. Persistent cases account for 75% of observed AFib patients [Cal+17].

SR can be restored with a procedure class called Cardioversion (CV), a common implementation of which is electrical CV. Here, a strong impulse is used to depolarize all the tissue in the heart at once. Electrical CV has a success rate — restoring SR in the patient — of about 65% [Kup+09]. However, usually AFib within days to weeks. Therefore, as a proxy to AFib treatment success, often other endpoints are used — most commonly $\geq$ 12-month AFib recurrence, adverse clinical effects (including mortality), and Quality of Life (QOL). CV has a 12-month recurrence of approximately 85% [Sin+05]. This makes it an unsuitable treatment strategy for most patients when used alone. However, because of its high success rate of immediate conversion, it may be useful if SR can be maintained by other means.

The two most common treatment strategies for maintaining SR are Antiarrhythmic Drugs (AADs) and Catheter Ablation (CA). With current methods, they promise comparable success rates. The recent CABANA [MD+19; Mar+19] study examined multiple endpoints in a randomized controlled trial to compare contemporary clinical effectiveness. For AAD and CA, respectively, a 3-year recurrence of 69% vs 50% and all-cause mortality of 5.3% vs 4.7% were found. Additionally, they reported significant improvements of QOL in CA over AAD. The study largely confirmed previous smaller studies [Mar+18; Mor+14; Pac+13; Wil+10; Cos+12]. Currently, the European Society of

Cardiology (ESC) recommends patient choice [Cam+12] as the primary indication for an AAD versus CA treatment strategy. Only when AAD therapy fails is CA specifically indicated.

However, it is hypothesized that both treatment strategies can be further optimized. For AAD therapy, better-suited agents with higher success rates and fewer side effects may be prescribed [KR20]. Briefly, there are two classes of AADs: rhythm control, in which AFib is suppressed in the atria, and rate control, in which conduction of excitation through the Atrioventricular (AV) node is suppressed. A more complete description and classification has recently been published in [Lei+18].

For CA, different ablation strategies can be used. Commonly, the first-order procedure is Pulmonary Vein Isolation (PVI). In this procedure, an ablation catheter is inserted into the left atrium and used to destroy the tissue surrounding the Pulmonary Veins (PVs) to electrically isolate the rest of the atrium from them. The procedure has a 12-month recurrence rate of about 50% for persistent AFib, and about 40% for paroxysmal AFib [Gai+08]. For some patients, PVI may be repeated in a subsequent procedure if tissue reconnection has occurred some time after the initial isolation. Patients for whom PVI remains unsuccessful may require alternative strategies of atrial ablation. A non-exhaustive list of ablation strategies is described in section 2.2.

The most popular interpretation of varying CA / PVI success is described in the AFib driver theory. Here, localized myocardial tissue inside the atria or PVs is thought to *drive* AFib by either initiating electrical impulses similar to the SA node (commonly referred to as a **focal impulse**) or facilitating an electrical reentry circuit (commonly referred to as a **rotor**). Details are described in section 2.1. This theory accurately predicts that some drivers can be electrically isolated from the atria with a PVI - thereby nullifying their effect on ventricular contractions - while others (atria-situated) remain unaffected.

Research investigating measurable effects of driveres located in the PVs versus elsewhere in the atria remains limited. Previous efforts have largely focused on guiding treatment strategy and identifying atrial drivers. Their findings are discussed in chapter 2.

However, information on the presence of different driver types is valuable prior to ablation: It can be used to guide treatment strategy, predict treatment success, or stratify patients into subgroups for more informed analysis. A method is needed that can infer inner myocardial state without an invasive intervention, while ideally being as inexpensive and quick to collect in daily clinical practise as the standard 12-lead Electrocardiagrams (ECGs).

For targeted driver ablation, Electrographic Flow (EGF) [Bel+18] is a novel approach to interpreting voltages from dense intracardiac catheter electrode data. EGF maps are computed using a motion estimation algorithm commonly used in computer

vision tasks (Horn & Schunck [HS81]). A study testing the efficacy of EGF-guided targeted driver ablation is currently underway. EGF and related studies are discussed in section 2.4.

EGF-related techniques have not yet been tried on body surface data. However, it is well known that topological Body Surface (BS) ECG data yields important information about myocardial state [Ram+04], even if inverse mapping to intracardiac data is not easily achieved. I therefore hypothesize that when mapping atrial flow from body surface electrodes, phenomena similar to those observed in intracardiac data may also be observable.

Outline In this thesis, I use EGF-derived metrics extracted from dense unipolar BS ECGs to predict the presence of atrial drivers. Since ECGs are common and non-invasive, they can be collected and analyzed inexpensively. The studied metrics are derived from two knowledge sources: First, knowledge is drawn from previous recurrence prediction studies (section 2.3). Second, driver indications from intracardiac data, as described in previous research (section 2.4), are used as primary assumptions for EGF-based metrics. A list of metrics derived and tested in this thesis is described in section 4.3.

Knowledge of the presence of atria-situated drivers would indicate the need for a non-PVI treatment strategy and should therefor correlate positively with recurrence. By testing this hypothesis, this thesis can hopefully contribute to effective low-cost stratification of patients prior to invasive intervention for treatment guidance and further research.

2 State of the Art

Because atrial fibrillation is such a common yet consequential and complex disease, it has long been the subject of extensive research. Knowledge of the disease is confirmed in most of recorded history [Faz07], with the appropriate attribution to the circulatory system dating back to 1628. The first human AFib ECG was recorded in 1906, and shortly thereafter in 1921 [LDI21], the theory of AFib drivers was proposed. Current formulations and open questions about drivers are discussed in section 2.1.

At the time, it became clear that further interpretation of AFib by pure expert knowledge had limited success. Recurrence prediction, among other endpoints, was achieved with better success rates when metrics based on clinical patient history were used. However, even these encountered severe limitations in effectiveness. This class of metrics is discussed in detail in section 2.3.

Only recently did ECG-derived metrics regain popularity, with the advent of fast and easily accessible computing power. Predictions based on automated sample-based metrics achieved high predictive success, outperforming those based on clinical patient history. One such metric, AFib amplitude, generally predicts spontaneous termination of AFib during ablation with a sensitivity of approximately 80% and a specitivity of 70% [Nau+09].

However, this simple baseline metric still serves as the cornerstone of ECG-derived metrics. It is likely to reflect the general state of the atrium, correlating with atrial fibrosis [Nak+19]. This suggests that the ECG may offer undiscovered potential for further stratification or analysis of AFib patients. ECG-derived scores are described in subsection 2.3.1.

In this thesis, body surface EGF maps are introduced. As such, EGF and the evidence supporting EGF in intracardiac data need to be discussed (section 2.4). The applicability of EGF on the body surface has not been previously tested and is the subject of this thesis.

2.1 Drivers of Atrial Fibrillation

The concept of atrial fibrillation drivers describes localized myocardial tissue that perpetuates ("drives") a patient's atrial fibrillation. Two different types of drivers can

be observed: **foci** and **rotors**. In the following section, I briefly describe a contemporary understanding of AFib drivers. A more complete description has recently been described elsewhere [Man+18].

Rotors, also called reentrant drivers, are localized tissues that facilitate micro reentry circuits (Figure 2.1). They function analogously to macro reentry circuits, in which larger structures facilitate reentry — often sustaining regular tachycardia — but due to the complexity of AFib wavefront propagation and size of the circuit cannot be observed as easily.

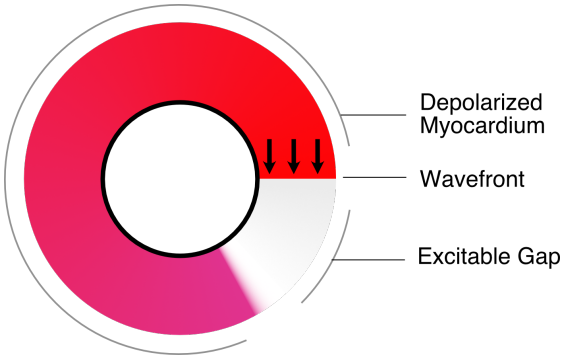

Figure 2.1: Simplified rotor reentry circuit. A wavefront propagates around an effective electrical blockage (e.g., a scar) more slowly than repolarization. Note that there is not necessarily a blockage to the surrounding tissue, so the wavefront can propagate outward.

Foci, also called focal impulses, are localized tissues that act as ectopic pacemakers, effectively similar to SA nodes. Many cells have the capacity for automaticity, but are normally suppressed by the higher rate of the SA node.

It is likely that both of these drivers exist and contribute to the maintenance of AFib. In some cases, both types of drivers have been observed in the same patient [Til+20]. In general, however, ground truth knowledge about the existence and contribution of each in individual patients is sparse and subject to a lot of contemporary research. It is likely that better understanding and knowledge of the presence of these drivers can help guide treatment strategies and provide insight into long-term outcome.

Both types of drivers have been described to generally switch on and off at irregular intervals [Cuc+10], possibly contributing to the complex nature of AFib. Some drivers may be active more frequently or for longer periods, while others are entirely transient and likely contribute little to the maintenance of AFib. Identifying the primary sites is key to understanding a patient's AFib.

To support the driver theory, many contemporary studies suggest that atrial fibrosis

plays a primary role in the maintenance of AFib [McG+14; Lau+17; Pla17; Sah+18]. In addition, areas of fractionated signal indicate slow conduction and may serve as fulcrums for complex reentrant circuits [Nad+04].

An adjunct to driver theory that must be considered is the possibility of transmural conduction. Here, the myocardium is modeled as consisting of *multiple layers* (multilayer hypothesis). This opens the possibility of rotational sites orthogonal to the surface of the myocardium, facilitated by reentry circuits breaking through different layers of myocardium. Some mapping techniques would observe this type of rotor as a focus, in particular if bipolar electrodes are used. However, elimination of these epicardial breakthroughs by ablation would provide a similar result to ablation of a micro reentry circuit or focal source, potentially terminating AFib.

There are other interpretations of possible factors, and indeed, multiple factors may ultimately contribute to sustaining AFib. The leading counter theory to localized AFib drivers is the meandering wave theory: this postulates that multiple meandering waves maintain AFib and no single focus or rotor is active for a sustained period of time. This theory has fallen out of favor due to increasing evidence supporting AFib drivers [Til+20]. In an example of contrasting observations, Sahadevan et al. [Sah+04] collected dense electrode data (404 electrodes) from 9 patients simultaneously in both atria (8/9) during open heart surgery. They found localized sites of stable, repetitive activation (7/9) and postulated that these served as drivers.

2.2 Targets of Atrial Ablation

In general, the efficacy of ablation techniques is difficult to assess because desirable endpoints [Cal+17] are often elusive, require long waiting times or are inherently fuzzy. This is further complicated by the fact that there are many modalities for ablation treatment: e.g. the target, the isolation technology, or even simply the tested endpoint. For optimal treatment, ablation techniques may need to be selected on a patient-specific basis and a one-fits-all solution may not be realistic. However, meaningful stratification for this has yet to be defined.

In the following section, different approaches to ablation targets are reviewed. These may help to illustrate the diversity of the AFib treatment landscape and provide insight into past or current interpretations of the nature of AFib and the role of various factors in its maintenance.

A long standing ablation strategy is linear line ablation. This procedure involves the creation of single long ablation lesions along the atria. While somewhat effective when performed as a singular measure [Wu+14], it has more recently been shown to provide no additional efficacy when performed in addition to PVI [Zhi+16].

Cox et al. performed the first maze ablation (also called 'cut-and-sew' maze ablation) [CSB00] in 1987. This procedure involves a series of long surgical lesions across the myocardium that create electrical blocks and inhibit free flow across the atria. It was long considered the "gold standard" of ablation treatment. A detailed contemporary understanding of the technique has recently been described in [Rua+18]. Later in 1994, the same technique was performed using CA [Sch+82] which facilitated closed-heart interventions [Swa94]. Ablations using CA while performing the same lesions are often referred to as 'mini-maze' ablations. A remaining advantage of surgical ablation is that the transmurality and completeness of lesions can be assured [Stu+07].

In 1998, Haïssaguerre et al. posed and tested the hypothesis of spontaneous initiation of atrial fibrillation by ectopic beats originating in the pulmonary veins [Haï+98]. They studied AFib patients in SR and mapped the point of earliest activation preceding an initiation of AFib. They confirmed the accuracy of their prediction by testing whether AFib terminated after ablation of the focus. Following this publication, PVI emerged to clinical practice as a minimal and effective procedure, where the PVs are electrically isolated from the rest of the myocardium. PVI is currently considered by many to be the staple procedure for CA, and is usually performed in all patients before other ablation strategies are considered.

In a more recent metastudy, Nery et al. [Ner+16] evaluated 11 studies on the association between reconnection of PV tissue and AFib recurrence. They found that electrical reconnection around at least one PV occurred in 58.6% of the AF-Free population and in 91.2% of the recurrent population. This suggests that reconnection of tissue is common even in nonrecurrent patients, although even more common in patients without a favorable outcome, and that complete isolation of all PVs may not be required in all patients. At the same time, complete isolation does not guarantee freedom from AFib at follow-up, suggesting the involvement of other mechanisms in at least these populations. They concluded that further research is needed and raised the question of whether the high effectiveness of AFib is solely attributable to the electrical isolation of ectopic foci.

However, even after the establishment of PVI as the cornerstone of ablative AFib treatment, other ablation targets have been proposed to determine whether this technique can be surpassed, or to provide an alternative for patients for whom PVI remains unsuccessful.

The 2012 CONFIRM (Conventional Ablation for Atrial Fibrillation With or Without Focal Impulse and Rotor Modulation) [Til+20] trial was the first to investigate the effectiveness of adding targeted atrial driver ablation to conventional ablation procedures. Conventional procedures here entailed a PVI and possibly additional linear ablations, added at the discretion of the treating physiologist. Their primary acute endpoint

was the modulation of AFib (expressed as spontaneous termination or prolongation of AFib cycle length during ablation). They observed a modulation in 86% vs 20% of their patients for the acute endpoint. For another endpoint, a 1 year followup of AFib, they observed a 45% vs 82% recurrence, suggesting localized drivers as an appropriate ablation target.

Another potential ablation target are Ganglionated Plexis (GPs). Here, four GPs that are located near the PVs are ablated. Po et al. [PNJ09] showed improved clinical outcomes when GPs were targeted in addition to the PVs, although success rates varied depending on the performing sites.

The most commonly used treatment avenues for AFib are currently AADs and PVI. The largest related treatment outcome study, the CABANA [MD+19; Mar+19] trial reported evidence for PVI outperforming AAD treatment. For AADs and PVI, respectively, they reported a 3-year recurrence of 69% vs 50%, all-cause mortality of 5.3% vs 4.7%, and significant improvements of QOL in CA over AAD. The study largely confirmed previous, smaller studies [Mar+18; Mor+14; Pac+13; Wil+10; Cos+12].

As market share of CA grows, so will research investigating ablation techniques, and in particular, targets of ablation. If driver theory proves itself and is supported by new data, it is likely that future methods will shift more toward targeted driver ablation to increase treatment efficacy and minimize myocardial destruction, which can lead to stiff atrial syndrome [Yan+16].

2.3 Atrial Fibrillation Risk Scores

When labeling recurrence, there is a general consensus that prolonged and more rigorous monitoring is often required to detect AFib. Indeed, many procedures lower the AFib burden, sometimes to a point where it is no longer perceptible to the patient — even when AFib subsists in the atria. This can still lead to further negative clinical outcomes, especially since AFib is a progressive disease. A 2017 consensus discusses several potentially relevant endpoints [Cal+17]. However, many trials do not or cannot meet high monitoring standards, and simpler labels are common - subsequently overestimating success rates. This can be a particular challenge when designing recurrence predictors.

Several clinical risk scores for recurrence of AFib in patients have been proposed in the past. However, the performance of scores using only information based on clinical patient history is inconsistent and limited [Dre+20]. Nevertheless, some factors appear in many different scores and therefore appear to be at least somewhat relevant. The metastudy by Dretzke et al. postulates that other factors may be needed to achieve better predictions, such as ECG, imaging-based, or genetic. The most common predictors

in these clinical scores, listed by how many scores included them, were left atrial parameters (9/13), type of AF (8/13), age (7/13), sex (4/13), and Estimated Glomerular Filtration Rate (eGFR) (4/13). Among other predictors were duration of persistent AF, current smoking, AFib history, early recurrence, and hypertension.

Kim et al. [Kim+20] used a neural network on 527 consecutive patients to predict AFib recurrence. The inputs to the network were purely clinical, with the exception of Left Atrial (LA) volume and 3D reconstructed LA images. They obtained comparable results to existing scores (Area under Curve (AUC)= 0.61) and concluded that a larger scale study is required.

It is likely that clinical factors alone will not be sufficient to build a meaningful stratification of the patient landscape. However, none of these scores consider the treatment type as an additional measure of possible success rate. Depending on the type of patient type, it is possible that different metrics may better indicate risk depending on the type of treatment chosen, given that factors contributing to a patient's AFib may vary by patient. Unfortunately, these mechanisms are not well understood, and knowledge of the exact contributors to AFib maintenance in individual patients is difficult to obtain. Therefore, this possibility has not been widely explored and should be considered for future risk scores or recurrence assessments.

Some AFib recurrence risk scores that incorporate more than purely clinical data have been proposed. An example was proposed by Shade et al. [Sha+20], who used Late Gadolinium Enhanced Magnetic Resonance Imaging (LGE-MRI) to create a personalized computational model of the left atrium. They then extracted features from both raw images and simulations of AFib induction to feed into a machine learning model. The model was used to predict recurrence risk. It was found that the induction simulations had high predictive power (AUC = 0.82), while the raw images did not (AUC = 0.47). The classifier predicted the probability of AFib recurrence with an average validation sensitivity of 82% and specificity of 89%.

2.3.1 Risk Scores derived from Electrocardiography

Although it is a useful analytical tool that can provide a wealth of information about various factors of the circulatory system, the ECG did not initially prove particularly useful in atrial fibrillation. The complexity of AFib signals makes it difficult to interpret the superimposed signal of wavefronts and other components by eye.

However, ECG has recently found a resurgence in popularity using more complex, automated, and technical algorithms for interpretation rather than expert knowledge. Promising results have been obtained and have proven that the ECG provides important information about the nature of AFib. Both analytical time series signal processing models and machine learning models have been proposed for data interpretation.

In 2004, Electrocardiographic Imaging (ECGI) was presented [Ram+04]. Here, 224 ECGs were collected from a vest on the torso. Computed Tomography (CT) scans and data from these electrodes were then used to reconstruct electrical potentials, electrograms and isochrones on the heart surface using mathematical algorithms. This work proved the relevance of dense electrode data and demonstrated its ability to provide important information about patients.

In 2010, Cuculich et al. used ECGI to characterize AFib patients [Cuc+10]. Using the CARTO system as ground truth, they reported that they were able to map low-amplitude signals with high accuracy. They observed multiwavelet reentry in most patients. Rotor activity was seen in only about 15%, focal activity near the PVs in 69%, and other focal sources in 62%. Other recent studies also reported on insight and ablation guided by this technology [Yam+15; Kne+17; Hai+14].

The above studies use a class of techniques that attempt to solve the inverse problem of electrocardiography. This problem space is considered by some to be underdefined [Oos03] and ill-conditioned [Oos12]. In addition, dense electrode vests also have intrinsic limitations: They are expensive, tend to have low adhesion, and are generally impractical, so other techniques have been proposed to overcome these technical limitations or to reformulate questions in more appropriate problem spaces.

In 2008, Nault et al. [Nau+09] demonstrated the predictive power of Fibrillatory Wave (F-Wave) amplitudes for recurrence. This metric is still widely considered the most powerful currently measurable metric from single-lead ECGs. In addition to recurrence, it correlated with AFib duration and patient age. A maximum amplitude of ≥ 0.07mV predicted termination of AFib by ablation with a sensitivity of 82% / 79% and a specitivity of 68% / 73% in leads V1 / II respectively. 43% of patients with mean f wave amplitude < 0.05 in lead V1 experienced AFib recurrence compared to 12% of those with F-wave ≥ 0.05 ($p = 0.004$). The metric has been found to be temporally stable by other studies [Xi+04; Meo+15].

Lankveld et al. examined other parameters derived from 12-lead ECGs for their predictive power for long-term catheter ablation success and spontaneous termination during ablation [Lan+16]. The studied parameters included both frequency-space (dominant frequency, organization index, spectral entropy) and time-space (F-Wave amplitude, sample entropy) metrics. They confirmed F-Wave amplitude as the best predictor. Their combined model achieved a validation set AUC $= 0.61$ for recurrence, and AUC $= 0.70$ for termination.

Luongo et al. [Luo+20] ingested simulated 3-second ECG data to extract several parameters from 12-lead sampled ECGs. For the simulation, transmural fibrotic tissue was modelled as 2 circular patches with a radius of 14 mm in which 50% of the elements were not conductive and the other 50% included ionic changes to represent the effect of cytokines. Singularities were then placed at uniformly distributed points in the atria.

Of 3 classes, 5 features were found to be especially statistically significant: Recurrence quantification analysis on vectocardiogram (entropy of the diagonal lines, laminarity), ratio Principal Component Analysis (PCA), eigenvalues (Standard Deviation (STD) over segments), and reduced lead spatial Recurrence Quantification Analysis (RQA) (entropy of the vertical lines, determinism).

They proposed a decision tree classifier using 3 of these features to predict the location of an atrial driver to be near the PVs or elsewhere in the atria. On simulated data, the classifier achieved a test set accuracy of 98.5%, specificity of 100%, and a sensitivity of 83.3%.

2.4 Electrographic Flow Mapping

EGF is a novel approach to map AFib conduction across the atrial surface. It was proposed and described in detail in 2018 [Bel+18]. Briefly, an EGF flow map represents the inferred wavefront propagation directions within a given time period as a 2D vector field. An example of different sites as observed in EGF maps can be seen in Figure 2.2.

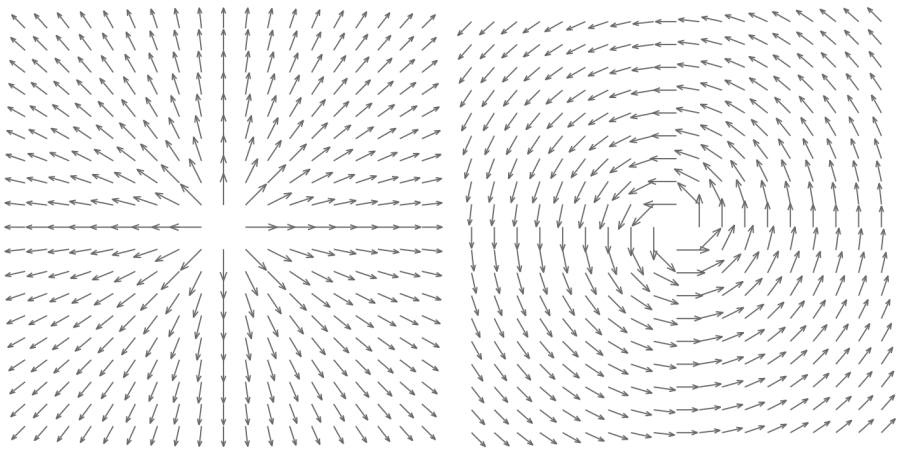

Figure 2.2: Perfect simulated focal (left) and rotational (right) sites in an EGF map. Flow is represented as vectors in a plane.

It is worth noting that, in EGF maps, rotational sites may be observed that are not divergent (Figure 2.3). When searching for sources, both divergence and rotation must be considered in order to classify singularities.

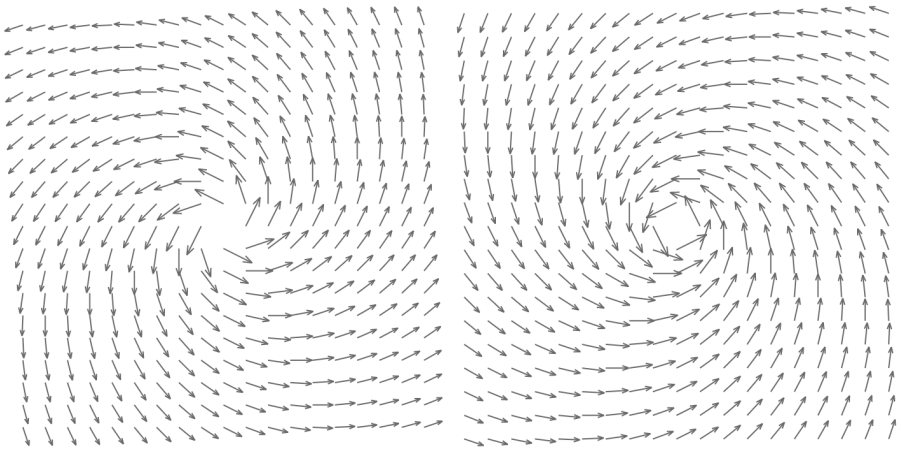

Figure 2.3: An example of a divergent (left) and convergent (right) rotational site. A convergent rotational site is not a true rotor, since wavefronts must logically propagate from it if it drives atrial fibrillation.

To compute EGF, the atrial signal is first separated from other superimposed component (e.g. noise, ventricular far-field, baseline wander). Additional processing steps may be applied, such as downsampling or filtering. The multilead data is then projected onto a 2D texture and interpolated to a higher resolution. Finally, an adaptation of the algorithm introduced by Horn & Schunck [HS81] is computed on the texture. This algorithm formulates visual motion as a minimization problem of vector lengths and spatial uniformity. A detailed description of EGF computation can be found in section 4.2.

Bellmann et al. investigated the role of velocity in EGF maps [Bel+19]. They found that velocity was higher when the source under study was more stable. Additionally, catheter ablation reduced the source stability, suggesting a possible role for these parameters during ablation.

Swerdlow et al. compared EGF with another source identification technique, phase mapping [Swe+19]. They found that sources were identified in a similar number of patients (81% and 83% for EGF and phasemapping, respectively). The methods complemented each other, with only 2% of patients having no source identified by either method. Overall, EGF identified more localized sources than phasemapping, with a higher prevalence of focal sources versus rotors (49% vs 2%, $P < 0.01$).

There is no previous work on EGF generated from body surface ECGs.

3 Body Surface Electrode Datasets

To design the pipeline, as well as to evaluate its effectiveness, human AFib ECGs were used from 2 different datasets. In this section, these are presented, analyzed, and discussed. A total of $25 + 100 = 125$ patients were available for analysis.

Both datasets are similar in nature. Patients were recorded using a dense BS ECG setup on the torso. Then, the patients were treated with PVI. Note that some patients were not "de novo" — meaning they may have undergone prior unsuccessful treatment. Some patients were also treated with additional ablation lines and medications.

3.1 Dataset A

Dataset **A** is an uncontrolled *prospective* dataset of 25 patients collected in collaboration with the Klinikum der Universität München.

Here, a custom electrode placement was designed using 8 individual 8-electrode strips. The strips were arranged in an equidistant configuration around the torso (Figure 3.1). Electrode data were collected using a commercially available amplifier (TMSi Refa), and consecutive 30 minute recordings were made. Patients lay supine and were instructed to limit their movements during the recording. Digitally, electrode positions were assumed to align with a perfect cylinder. Ground truth locations may differ slightly due to manual electrode placement.

Later, these recordings were divided into disjoint 1-min recordings for analysis. The leads were manually checked for quality (e.g. dead leads, poor adhesion, noise) during recording, and the setup was adjusted until a clean recording could be obtained.

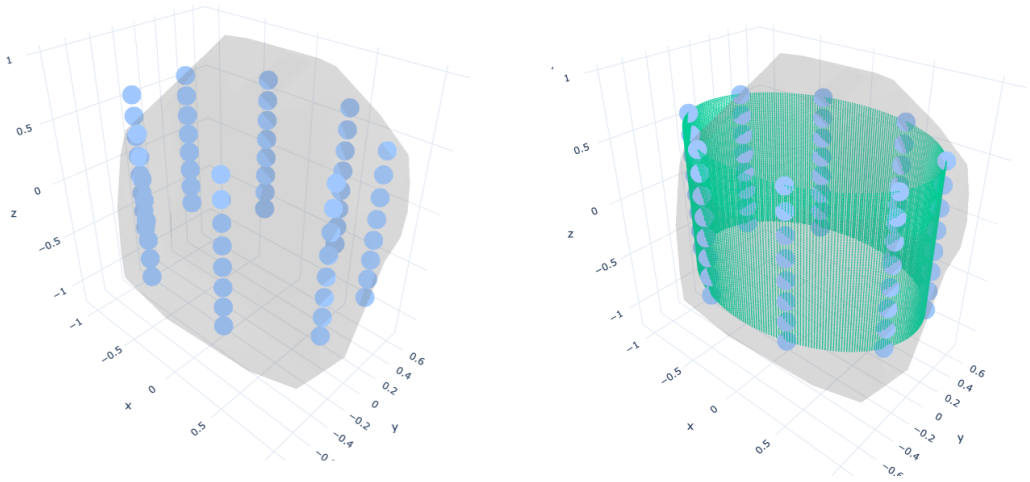

Figure 3.1: Systematic electrode locations along the torso of a patient in dataset **A**. A 3D scan of a patient's torso is shown in grey. In the second image, texture positions that are later interpolated are overlaid in green.

Subsequently, a PVI was performed. In rare cases, additional ablation lines were performed at the discretion of the treating physician. Similarly, some patients later received additional drug treatment if treatment was unsuccessful. A 3-month and 12-month follow-up of recurrence was collected using a remote telephone questionnaire.

In an adjunct to to the 25 AFib-patient recordings, 7 recordings of healthy patients were created.

3.2 Dataset B

Dataset **B** is a *retrospective* dataset of 120 patients collected during commercial cases in Russia.

Here, off-the-shelf electrode strips (EP Solutions) were used to collect 240-lead ECGs for 30 consecutive minutes. These recordings were later divided into disjoint 1-minute recordings for analysis. In addition, leads were manually assessed by clinicians to identify outliers (e.g. dead leads, poor adhesion), which were excluded from analysis.

Subsequently, PVI was performed by radiofrequency ablation. If spontaneous termination of AFib did not occur during PVI, it was at the discretion of the treating physician to perform additional ablation lines. Similarly, if treatment was unsuccessful and patients had an early recurrence, some later received additional drug treatment.

All patients received oral anticoagulants ($n = 33$ Apixaban, $n = 41$ Xarelto, $n = 46$ Pradaxa). A 2-week and 12-month recurrence followup was collected.

Electrode positions were provided with with euclidean coordinates (Figure 3.2).

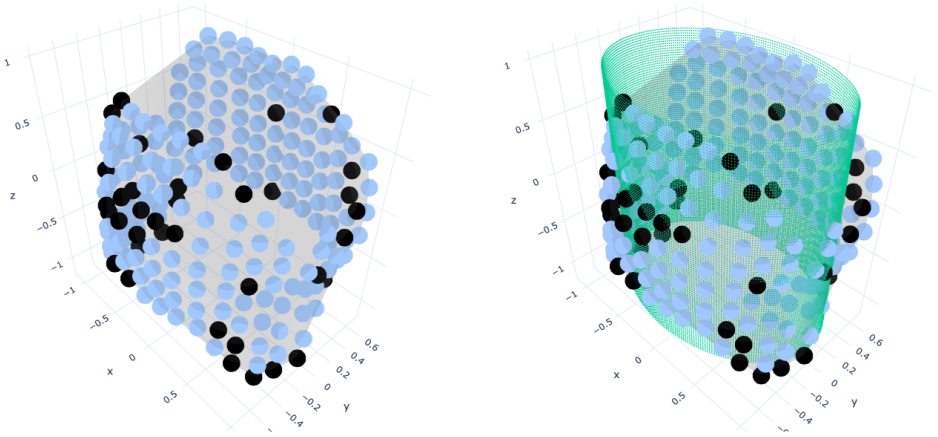

Figure 3.2: Example of derived electrode positions along the torso of a patient in dataset **B**. Some electrodes were marked as invalid and excluded from the analysis - these are colored black in the image. In the second image, texture positions that are later interpolated from the source data are overlaid in green.

3.3 Descriptive Analysis

This section presents the purely descriptive characteristics of the datasets in Table 3.1. The prospective dataset **A** includes 25 patients, while the retrospective dataset **B** includes 120, to a total of 145 analyzed patients. Respectively, datasets **A** and **B** include a ratio of 96.0% vs 88.3% (89.7% overall) patients diagnosed with persistent AFib, and report a 12-month recurrence of 40.0% vs 46.7% (45.5% overall). This is similar to expected values for this type of procedure.

Metric \ Dataset	A	B	Overall
Electrodes	64	≤ 240	
Patient Count	25	120	145
Sex			
Female	6 (24.0%)	43 (35.8%)	49 (33.8%)
Male	19 (76.0%)	77 (64.2%)	96 (66.2%)
Other Medical Attributes			
Age	68.1 ± 12.3	62.6 ± 9.4	61.9 ± 10.3
Height (cm)	173.3 ± 17.8	174.1 ± 9.2	173.9 ± 11.1
Weight (kg)	87.0 ± 18.9	91.0 ± 19.1	90.3 ± 19.1
BMI	30.4 ± 15.1	29.9 ± 5.3	30.0 ± 7.8
LA Volume (ml)	196.5 ± 66.5	*unavailable*	-
LAA Volume (ml)	*unavailable*	104.1 ± 26.8	-
Medical History			
Persistent AF	24 (96.0%)	106 (88.3%)	130 (89.7%)
Ablation			
Spontaneous Termination	*unavailable*	39 (32.5%)	-
No Additional Ablations	*unavailable*	60 (50.0%)	-
+ LA Posterior	*unavailable*	58 (48.3%)	-
+ LA Anterior	*unavailable*	21 (17.5%)	-
+ LA Inferior	*unavailable*	2 (1.7%)	-
+ Roof	*unavailable*	21 (17.5%)	-
Drugs			
Oral Anticoagulants	25 (100%)	120 (100%)	145 (100%)
Beta Blockers	*unavailable*	52 (43.3%)	-
Followup			
2 week recurrence	*unavailable*	35 (29.2%)	-
3 month recurrence	9 (36.0%)	*unavailable*	-
12 month recurrence	10 (40.0%)	56 (46.7%)	66 (45.5%)

Table 3.1: Properties of the datasets. ($x \pm y$ indicates the mean and standard deviation)

4 Methods

4.1 Isolation of Atrial Signals

Any ECG can be modeled as a superimposition of several independent components. It can therefore be expressed as such:

$$x = \sum x_{component} \tag{4.1}$$

Fortunately, the biggest contributors to the signal, in terms of amplitude, are well known:

- x_{atrial}: voltage differences originating from wavefronts in the atria.
- $x_{ventricular}$: voltage differences originating from wavefronts in the ventricles.
- $x_{baseline\text{-}wander}$: a low-frequency high-amplitude component originating from various sources including respiration, body movement, and poor electrode adhesion.
- x_{mains}: sinusoid component of narrow frequency bands originating from nearby electronic devices.
- $x_{far\text{-}field}$: other components of similar morphology in all recorded electrodes.

In this thesis, therefore, the signal decomposition is conceptually modeled as such:

$$x = x_{atrial} + x_{ventricular} + x_{baseline\text{-}wander} + x_{mains} + x_{far\text{-}field} + x_{unknown} \tag{4.2}$$

For atrial parameters, only the atrial component of the signal is relevant. The other superimposed components may interfere with the calculation, especially if they are of comparable or higher amplitude than x_{atrial}. Fortunately, because the biggest contributors to the signal in terms of amplitude are well-known, expert knowledge can be used to approximate their shape and subsequently subtract them from the final signals. However, since a perfect approximation is unlikely, an error term must be added. An attempt to separate atrial signals would therefore be modeled as such:

$$x_{atrial} + x_{unknown} + error = x - (\hat{x}_{ventricular} + \hat{x}_{baseline\text{-}wander} + \hat{x}_{mains} + \hat{x}_{far\text{-}field}) \tag{4.3}$$

In reality, however, atrial separation is usually achieved by applying several functions to the signal in sequence. These may change the morphology or even the phase of the signal. An example of a more appropriate model of actual separation may therefore be expressed as such:

$$\hat{x}_{atrial} = \text{rm\_ventricular}(\text{rm\_mains}(\text{rm\_baseline}(\text{rm\_farfield}(x)))) \tag{4.4}$$

In this thesis, as in most previous studies, isolation of atrial signals is achieved by several sequential processing steps. Therefore, there may be a change in the morphology of the individual components. The pipeline can be represented by the following simplified pseudocode:

```
# N = Number of channels
# T = Number of samples in each channel
# C = Number of qrs clusters
# ~L = Number of templates in a qrs cluster

def isolate_atrial_components(signal: [N, T]) -> [N, TS]:
    reference_signal: [N, T] = signal
    reference_signal = mitigate_mains_noise(reference_signal)
    reference_signal = highpass_filter(reference_signal)

    qrs_clusters: [C][~L] = templates.locate_clusters(reference_signal)
    mains_noise_hz: float = find_max_frequency(reference_signal)

    signal = zero_center_channels(signal)
    signal = subtract_global_average(signal)
    signal = mitigate_mains_noise(signal, mains_noise_hz)
    signal = cancel_synchronized_qrs(signal, qrs_clusters)
    signal = remove_baseline_wander(signal)
    signal = lowpass_butter(signal, hz=50)

    return signal
```

In the following subsections, each step is examined for its purpose, and the implementation is presented. Notably, there are many hyperparameters that are not represented in the simplified implementations provided here. Some of these are discussed in the respective sections; in general, these have been adapted on a case-by-case basis, taking into account expert knowledge, signal reproducibility, and optimization heuristics.

A complete example of the steps of atrial signal isolation can be found in section .1.

4.1.1 Zero-Centering

When a high-pass filter is applied to a signal that starts at an value, lateral ringing may occur depending on the cutoff frequency (ex: Figure 4.1). To avoid this, a zero-centering step is applied to each channel, shifting the entire signal by a constant without distorting it.

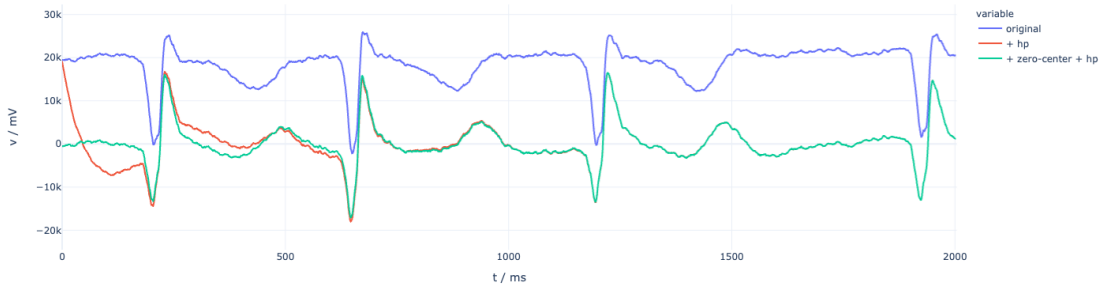

Figure 4.1: Zero-Centering: Example of morphology distortion / lateral ringing when a 2Hz high-pass filter is applied. Zero-Centering channels helps mitigate the effect.

```
def zero_center_channels(signal: [N, T]) -> [N, T]:
    return signal - signal[:, :100].mean(axis=-1, keepdims=True)
```

4.1.2 Global Average Subtraction

Signals often have some amount of far field from unwanted sources. By subtracting the average of all available channels from each, these effects can be mitigated.

```
def subtract_global_average(signal: [N, T]) -> [N, T]:
    return signal - signal.mean(axis=-1, keepdims=True)
```

4.1.3 Mains Hum Removal

Many recordings contain $50Hz$ or $60Hz$ noise as a superimposed signal. These may be electronic devices near the electrodes, the recording amplifier or the cables. The maginitude may vary, but if there is a systematic gradient between different recorded leads, it can induce flow in the flow estimation step. A good mains hum removal technique is required.

Previous works often used a notch filter. Notch filters are well-understood, commonly available and thus easy to employ. However, they have several disadvantages:

- Ringing can be induced in the start and end of the signal.
- If relevant signal covers frequencies in the same spectra, morphologies may be deterministically disturbed (Figure 4.2).

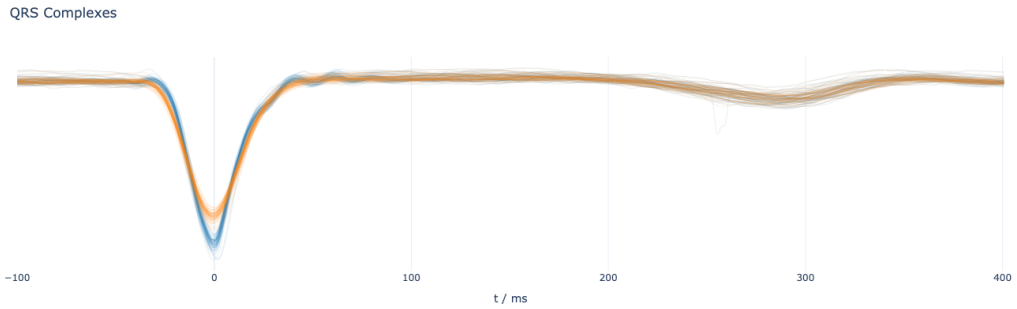

Figure 4.2: Example QRS-T morphology change when a 50Hz notch filter with a large frequency band is applied. Blue lines indicate individual QRS-T complexes before filtering. Orange lines indicate individual QRS-T complexes after filtering.

Because of this, other techniques have been proposed to remove mains noise [Gar+18].

Fortunately, these limitations can also be mitigated if the mains hum frequency is known to a high degree of precision. Frequencies of mains hums drift over time [], but not significantly within one minute. To achieve this, I implemented a mains frequency detection that decomposes the signal into frequency space using Fast Fourier Transform (FFT) and subsequently detects the largest peak in the range (49.9, 50.1). Evaluating the trade-off between a high degree of mains suppression and a morphology preservation, a notch filter size was determined that was found to be sufficient for this thesis.

4.1.4 Baseline Wander Correction

Many ECGs contain baseline wander as part of the superimposed signal. This term usually refers to low-frequency motion, the amplitude of which in many cases can exceed those of the desired signal by several factors. A common approach to removing this component is to use a high-pass filter. However, this has several disadvantages:

- Ringing may be induced in the beginning and end of the signal.

- The cutoff frequency imposes a trade-off of efficacy of the separation versus disturbance of morphologies.

These limitations are well-known, and other approaches have been proposed [Sun+19; GSJ15].

Recently, Wan et al. [Wan+19] proposed a method that combines two previous approaches, morphological and wavelet-based filtering, to create a more resilient model. Here, the signal is first simplified with morphological filters and then approximated with a Discrete Wavelet Transformation (DWT) low-pass filter. In this thesis, I use a similar strategy, with one adjustment: I replace the use of DWT with a more conventional bi-directional butterworth filter. These approaches are comparable, but in the studied data sets, the butterworth filter achieved more reliable results. A high-level pseudocode implementation can be described as follows:

```
def remove_baseline_wander(x: [N, T]) -> [N, T]:
    size = int(size_ms * sampling_rate_hz / 1000)
    size_t = (*(0,) * (x.ndim - 1), size)

    cl_op = grey_opening(grey_closing(x, size=size_t), size=size_t)
    op_cl = grey_closing(grey_opening(x, size=size_t), size=size_t)
    x_simple = (cl_op + op_cl) * 0.5

    baseline = lowpass_butter(x_simple, cutoff_hz=2.0)

    return x - baseline
```

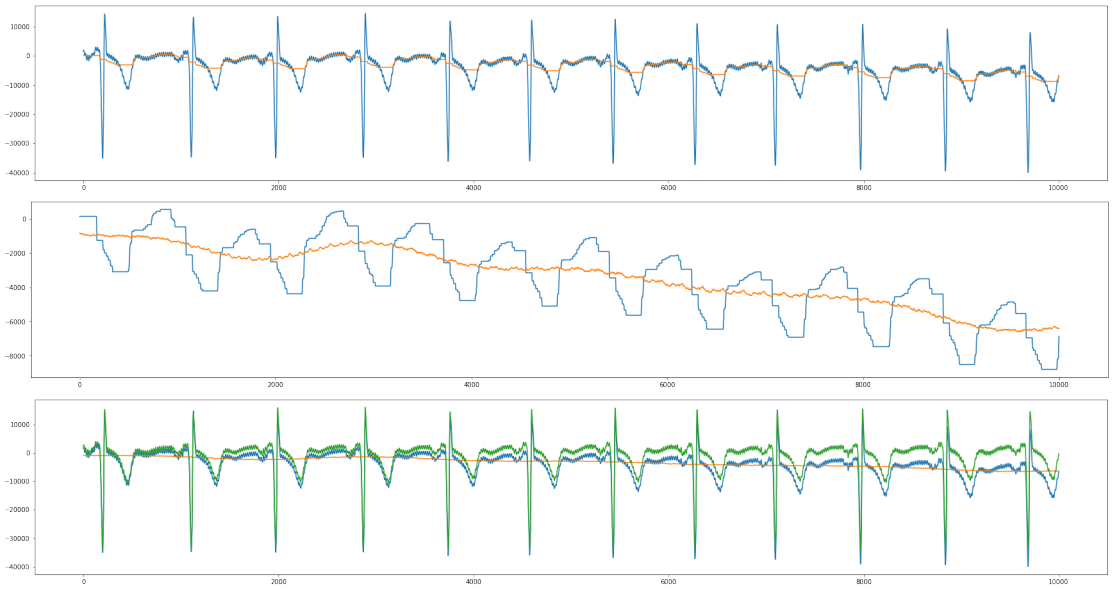

Figure 4.3: Example of baseline wander correction. The first diagram shows the original data (blue) and the simplified data (orange). The second diagram shows the simplified data (blue) and the low-pass filtered data (orange). The third plot shows the original data (blue), the estimated baseline (orange), and the corrected data (green). The x-axis represents milliseconds and the y-axis represents millivolts.

4.1.5 QRS-T Cancellation

Body Surface ECGs consist of several of superimposed signals, with the ventricular component usually posing by far the greatest influence in terms of amplitude. Depending on the placement of the electrode, this component may be more or less dominant, but when uniformly distributed electrodes around the torso are examined, one is dealing with a range of different morphologies and superimposition ratios. To properly isolate the atrial portions of a body surface ECG, the ventricular component must be removed to a high degree of accuracy. This is particularly important when using the underfitted Horn & Schunck method, as it is highly sensitive to repetitive systematic gradients.

Fortunately, given a sleeping or resting patient with steady breathing, morphologies of the QRS-T complexes can usually be considered to be very consistent — even in AFib patients. Moreover, in AFib patients, atrial activity is not synchronized to ventricular components (no AV-association). Thus, using templates, the repetitive ventricular component can be separated and finally subtracted from the signal. Similar approaches

have been used in previous studies with satisfactory results [KD07]. For this thesis, I have implemented and used a specially developed QRS-T cancellation algorithm that is capable of processing a wide variety of signals for reliable signal separation and ventricular component compensation.

This system builds templates with signal means and therefore requires sufficient baseline wander correction (e.g. through filtering) on its input signal (Figure 4.4).

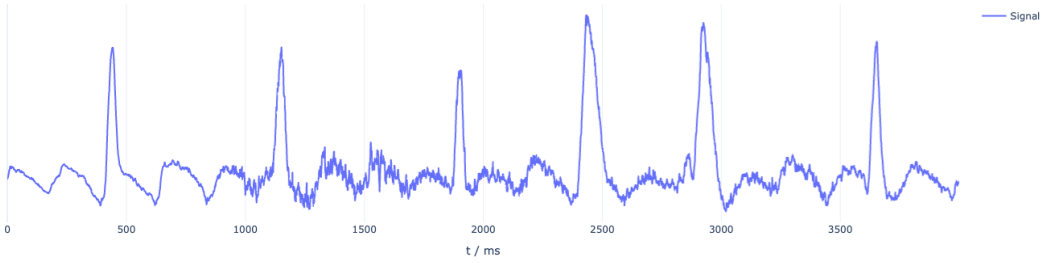

Figure 4.4: Input signal for ventricular signal separation.

Iterative Ventricular Component Estimation

While the baseline wander correction algorithm used in this thesis is excellent at preserving morphologies on the time axis, it can be somewhat inconsistent in estimating the baseline in terms of amplitude if high-amplitude QRS-T complexes exist in the signal.

This creates a problem: For precise QRS-T morphology estimation, the baseline must be properly corrected. However, for precise baseline correction, QRS-T complexes must be cancelled. Fortunately, the baseline estimation approach used is good at preserving morphologies on the time axis. This would not be the case for a conventional filter approach. This opens the possibility for an iterative approach, where each iteration can improve the estimations for each. The iterative approach converges after about 3 iterations.

The final signal with cancelled QRS can be obtained by simply subtracting the ventricular component from the original. Since QRS morphology is still somewhat variable, perfect separation cannot usually be achieved with this method. Therefore, the parts of the signal with the strongest slope (r-peaks) are excluded from further analysis (e.g. using a mask). An example of a complete QRS-T subtraction can be seen in Figure 4.5.

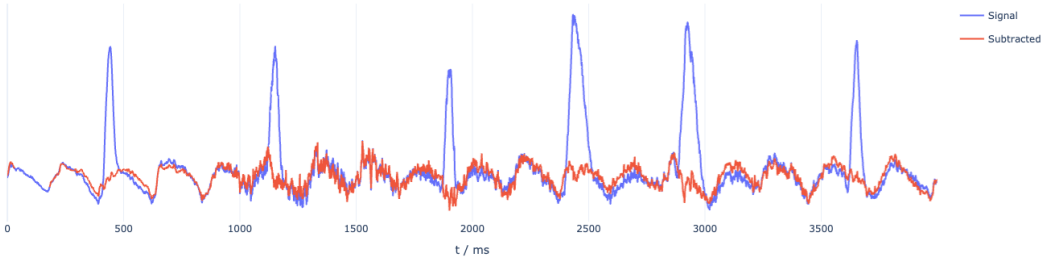

Figure 4.5: Isolation of non-ventricular signal by subtracting ventricular signal from the original.

A simplified pseudocode implementation can be expressed as such:

```
def cancel_synchronized_qrs(
    signal: [N, T],
    qrs_custers: [C][~L]
) -> [N, T]:
    ventricular_components: [N, T] = zeros_like(signal)
    for i in range(3):
        no_ventricular = signal - ventricular_components
        no_baseline = remove_baseline_wander(no_ventricular)

        ventricular_components += separate_ventricular(no_baseline)

    return signal - ventricular_components
```

Synchronization and Clustering

To create templates, timings and clusters must first be established. 3 steps are used to achieve this: The slope of the signal is analyzed to find local maxima (initial synchronization: Figure 4.6). Then, a window around each local maximum is converted to frequency magnitude space and input to the DBSCAN [Est+96] algorithm to form clusters. Finally, the timings of templates in each cluster are iteratively optimized using maximum correlation. This approach results in sub-millisecond and sub-sample timing accuracy.

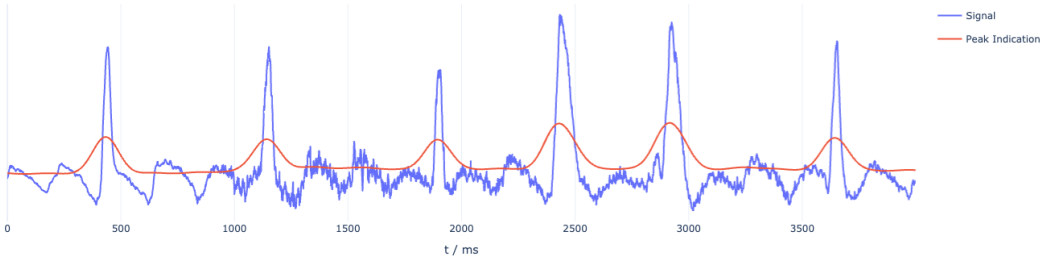

Figure 4.6: Detection of QRS instances by using the signal slope. The red line represents the amount of indication for a QRS, as computed using all channels.

Separation of Synchronized Signals using Templates

In sub-algorithm, timings are used to create templates that are then used to reconstruct the signal. First, for each channel and cluster, the signals synchronized at the QRS positions are superimposed. The templates are formed from the mean of the signals, with a minimum of 10 samples (Figure 4.7). If the signal is heavily prefiltered, different parts of the templates may blend into each other (e.g. T-Wave into QRS). To mitigate possible effects of other QRS-T instances in templates, a constant length ($n = 200$ms) before the R-Peak, and a variable length after the R-Peak (until the next influence window) is used to construct templates. This is especially important when the actual length of the T-Wave and heart rate are not precisely known at the time of the algorithm design, which is the case for any unsupervised algorithm.

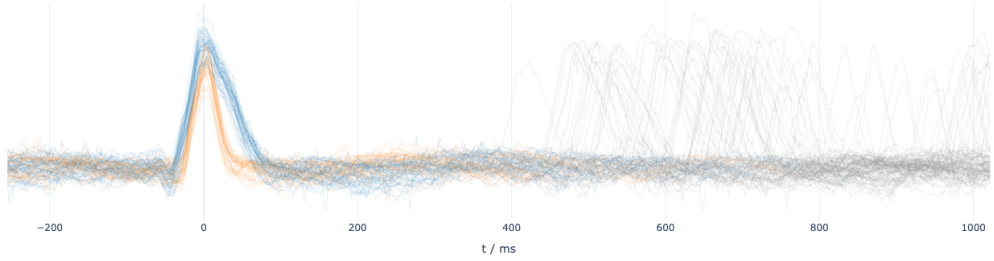

Figure 4.7: Superimposed clustered QRS-T instances for template construction. Each instance is drawn with a low alpha value so that the mean can be easily visually discerned. Gray lines represent portions of the templates that intersect the next QRS complex. The lines are otherwise colored according to their cluster as determined by the previous calculation step.

Finally, templates are inserted at the appropriate QRS locations (Figure 4.8). If

a template could not be constructed due to a low cluster size (e.g. for Premature Ventricular Contractions (PVCs)), corresponding parts of the signal are excluded from further analysis.

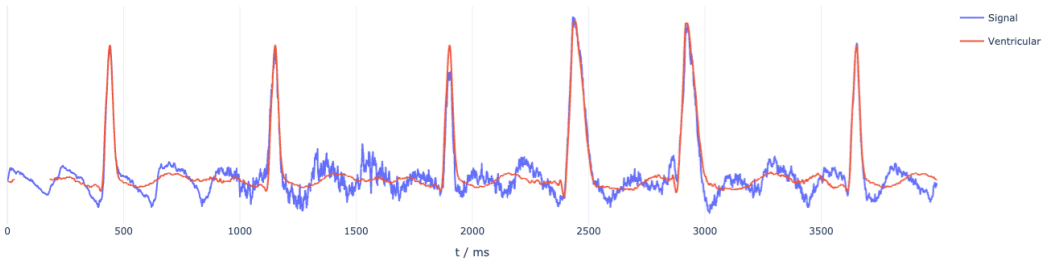

Figure 4.8: Reconstruction of the ventricular signal by insertion of templates. The blue line represents the original signal, the red line the reconstructed parts synchronised with instances of QRS.

4.1.6 Lowpass Filter

As a final step to atrial signal isolation, a low-pass filter is applied to the signal. Atrial components are known to be below 50Hz, and a low-pass filter can help eliminate outliers and artifacts introduced by earlier steps.

4.2 Flow Computation

To estimate atrial electrical flow, this work uses an adaptation of the visual flow estimation algorithm introduced by Horn & Schunck [HS81], but it must modify the data through several additional processing steps before it can be effectively applied. These steps are listed and explained in the following sections. Associated hyperparameters were manually optimized for reproducibility between independent recordings of the same patient and uniqueness between patients for all steps. The entire pipeline for flow estimation can be represented by the following simplified pseudocode:

```
# N = Number of channels
# T = Number of samples in each channel
# T2 = Number of samples after subsampling
# S = Number of segments
# F = Number of frames per segment
# R = Number of rows in the resulting texture
# C = Number of columns in the resulting texture

def estimate_flow(data: [N, T], positions: [N, 3]) -> [S, F, R, C, 2]:
    data_ss: [N, T2] = subsample(data, hz=1000 / 19)
    data_ss = normalize(data_ss)

    texture_shape: [R, C, 3] = shapes.cylinder.fit(positions, (R, C))
    data_projected: [R, C, T2] = resample_rbf(
        data,
        input_positions=positions,
        output_positions=texture_shape
    )

    data_segmented: [R, C, S, F+1] = split_into_segments(data_projected)

    return estimate_flow_hs(data_segmented)
```

4.2.1 Subsampling

Horn & Schunck's algorithm estimates flow based on spatial and temporal gradients from subsequent greyscale image pairs. The process of underfitting allows lower frequencies to be matched, but frequencies as high as the sampling frequency tend yet to dominate. In order to allow both higher computational speed and to increase the

scale of the analyzed frequencies, the signal must be subsampled. A sample length of 19 milliseconds is chosen for a high degree of reproducibility in flow maps. The resampling method chosen uses a windowed rolling mean to aggregate samples.

4.2.2 Normalization

The Horn & Schunck motion estimation algorithm assumes constant amplitudes in time and space ("brightness constancy assumption"). However, this is not the case for electrode-based data. In particular, electrodes placed on the patient's back record lower amplitudes than those placed on the front - but amplitudes can also vary over time. Therefore, a rolling window of amplitude estimation across each electrode is used to normalize the remaining signal. Notably, if there are no F-Waves in the signal, this will inflate either noise or possible residual values of previously separated signals (e.g. ventricular components). Therefore, high-quality separation of signals is required prior to this step. If unsystematic noise is inflated, the flow estimation algorithm will yield a low Flow Angle Stability (FAS) (described in subsection 4.3.1), which is usually interpreted as unsystematic flow and does not systematically affect any of the metrics analyzed.

4.2.3 Projection

Up to this point, the data have been considered as synchronized, but untopological time series. However, in order to compute Horn & Schunck, a 2D plane must be constructed. In addition, higher resolution is desirable to increase the smoothness of flow fields and possibly the accuracy of the metrics.

Fortunately, both can be achieved in the same step using Radial Basis Function (RBF) interpolation [BL88]. Here, positions are provided for each trace. An output shape is then defined, which are traces of equal shape and attached positions. For each time step and trace, the data is interpolated using a distance metric for weighting.

In this thesis, I use a cylindrical shape fitted to the input points as the input shape, since this shape can be easily unrolled into a texture. It is notable that when this shape is used, there is a rollover seam in the texture. This needs to be taken into account when calculating flow and subsequent metrics with kernels. I use euclidean distance as RBF's distance metric, and thin plate spline for interpolation. A simplified pseudocode implementation can be found below.

```
def resample_rbf(
    x: [N, ...],
    positions: [N, 3],
    texture_positions: [R, C, 3]
```

```
) -> [R, C, ...]:
    texture_positions_flat: [R*C, 3]
        = texture_positions.reshape(R * C, 3)

    wcm: [N, N] = weight_computation_matrix(
        positions
        distance_fn="euclidean"
    )
    rm: [R*C, N] = rbf_matrix(
        texture_positions, positions,
        distance="euclidean"
    )
    rm_wcm: [R*C, N] = rm @ wcm
    sample_values: [R*C, 1, ...] = rm_wcm @ data[:, newaxis, ...]

    return sample_values[:, 0].reshape(R, C, ...)
```

4.2.4 Segmentation

Because AFib drivers are transient and can spontaneously turn on and off at short intervals, the observed flow can strongly vary between independent time frames. Therefore, only short time windows (several seconds) are usually considered until the state is reset. If a driver is relevant to the maintenance of AFib, it should produce similar flow maps for independently considered time spans. Therefore, in this thesis, I segment the data into 2-second sections, using the data from the respective previous sections to initialize the flow field. A 60-second recording then yields $\left\lfloor \frac{60}{2} \right\rfloor - 1 = 29$ distinct flow fields and metrics. A simplified pseudocode implementation can be found below.

```
SEGMENT_SIZE_MS = 4000
OVERLAP_MS = 2000

def split_into_segments(x: [..., T]) -> [..., S, F]:
    stride_ms = SEGMENT_SIZE_MS - OVERLAP_MS
    segment_count_ms = (T - OVERLAP_MS) // stride
    return rolling(x, segment_count_ms, stride=stride_ms, axis=-1)
```

4.2.5 Frame-Wise Flow Estimation

To estimate flow, a commercial adaptation of the algorithm introduced by Horn & Schunck [HS81] is computed on the interpolated voltage texture frames (Ablacon, Inc.). This algorithm formulates visual motion as a minimization problem of vector lengths and spatial uniformity. In the adaptation, the flow vectors for each pair of frames are unterfitted so that many pairs can be input for the same vector field. As output, vector fields of the same size as the texture are produced; one for each window. Individual flow frames can also be analyzed for different metrics; however, due to the underfitting process, it is important to note that the vectors do not vary greatly from frame to frame.

4.3 Flow Maps

To evaluate flow calculation on the body surface, different techniques can be considered. In this thesis, I use three different methods that generate 2D feature maps of the same shape as the original flow maps. Example implementations of these methods pertaining to EGF in intracardiac data were provided by Ablacon, Inc. Some implementation details and hyperparameters were adjusted to optimize against computation on body surface data.

The resulting images (EGF maps) can be analyzed qualitatively or quantitatively in later steps. The calculation of flow frames and the subsequent flow estimation has already been discussed in section 4.2. The output of the flow function is twofold:

One, individual flow frames can be used to calculate subsequent maps and metrics. Due to the process of underfitting flow in this algorithm, successive flow frames are usually similar. This must be taken into account when analyzing flow using this data.

Two, full segments of flow can instead be used. Depending on the chosen segment size, these may represent several seconds of flow activity at once.

Based on the results of previous work with EGF and the assumption that drivers are transient and can turn on and off quickly, I evaluate metrics for individual flow frames in this thesis. Resulting maps are later aggregated over entire segments for computational simplicity. Thus, the number of resulting feature maps per recording is equivalent to the number of segments. The feature maps are created from a cylindrical approximation of the patient's torso. This texture unrolls from 3D space with $+y =$ superior and $+x =$ clockwise rotation. The left seam of the texture is at an angle of $\delta = -45^\circ$ to the anterior sagittal plane of the patient. This means that, in sequence, the left to right portions of the textures correspond to front, right, back, left sections of the patient's torso.

The techniques presented in this thesis are based on or inspired by phenomena often observed in flow maps of intracardiac electrode data, as described by previous research [Bel+18] — as well as contemporary knowledge about AFib drivers. In the following section, these are presented and explained.

4.3.1 Flow Angle Stability

Purpose

To locate and analyze areas of stable flow flow.

Background

In the intracardiac problem space, it has been shown that sources are usually surrounded by areas of stable flow. Similarly, it has been observed that flow is chaotic when an area is far from the nearest nearby source. Logically, this can be explained by the fact that the wave fronts originate from the nearby source, enabling little deviation. Far away tissue has a greater chance of accumulating differences in propagation patterns, and in addition meandering waves could further influence the flow. I therefore hypothesise that areas of high flow angle stability could be observed at the body surface if highly active sources are present in the atria.

Computation

FAS is calculated using flow angle frames as input. The mean values of all frame-pair differences per pixel are calculated. This substep is called flow angle total variation. An example calculation is shown in Figure 4.9. Flow angle stability values are then calculated using the equation $1/(x+\delta)$ where δ is an arbitrarily small number.

A pseudocode implementation based on a tensor for flow frames in cartesian vector representation follows:

```
def flow_angle_stability(flow_frames: [..., F, 2]) -> [..., F]:
    theta, _ = cartesian_to_polar(flow_frames.unstack(axis=-1))
    angle_diff: [..., F] = abs(theta[..., 1:] - theta[..., :-1])
    angle_diff = minimum(angle_diff, abs(angle_diff - 2 * pi))
    return 1.0 / (angle_diff.mean(axis=0) + 0.0001)
```

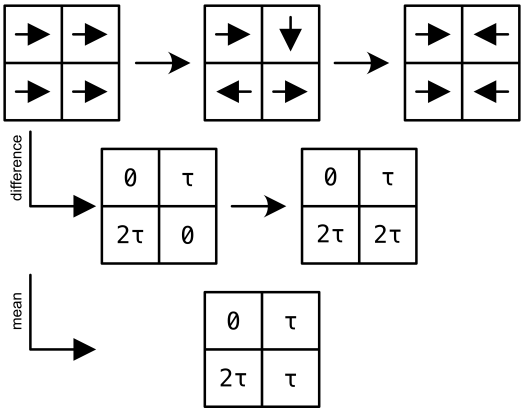

Figure 4.9: An example computation of a $2 * 2$ flow angle total variation map based on 3 consecutive flow frames.

Examples

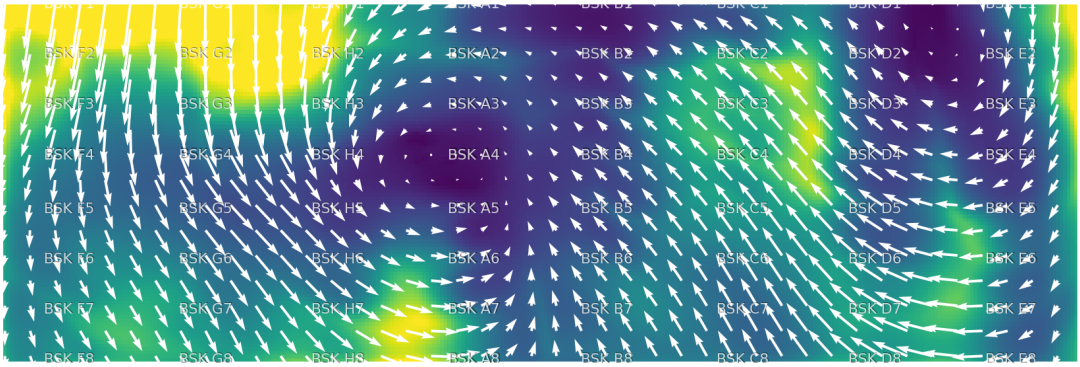

Figure 4.10: An example of a flow angle stability map, representative of 2 seconds of flow, of a patient in dataset **A**. Flow vectors and electrode labels are superimposed.

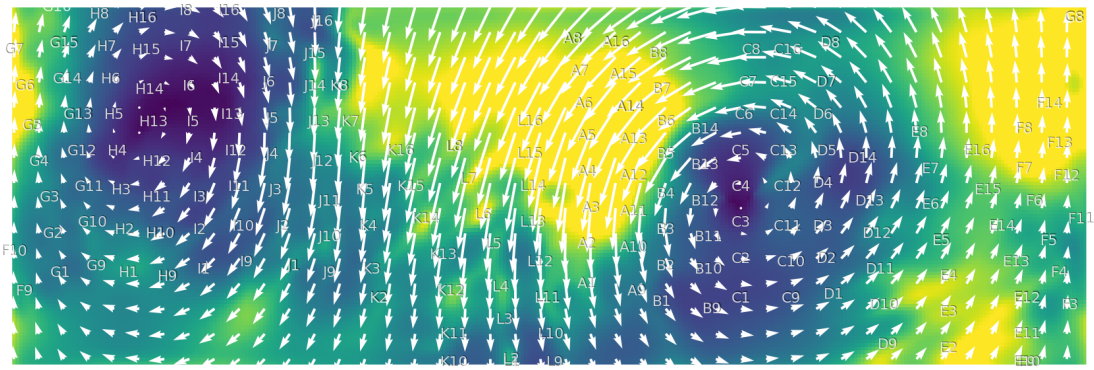

Figure 4.11: An example of a flow angle stability map, representative of 2 seconds of flow, of a patient in dataset **B**. Flow vectors and electrode labels are superimposed.

4.3.2 Streamline Origins Density

Purpose

To locate origins of wavefronts by quantifying divergent singularities.

Background

In the intracardiac problem space, sources have been shown to produce divergent flow patterns. Logically, this can be explained by drivers generating wave fronts that propagate outward. Divergence can be measured in several ways. One way is to simulate particles and move them in the reverse direction of flow. Areas where a high density of particles accumulates can be considered as divergent.

Computation

Streamline Origin Density (SOD) is calculated by simulating particles on a flow field.

The particles are generated at random, ideally at uniformly distributed positions. If the particles are moved along the flow field and converge to a singularity, sinks can be located. If the particles are moved along the inverted flow field and converge at a singularity, sources can be located. The complete motion vector from the source to the sink is called a streamline. Due to the smoothing term of the Horn & Schunck algorithm, singularities are unlikely to form randomly.

Finally, SOD is calculated by generating a texture, coloring the pixel closest to the singularity and finally smoothing the texture with a Gaussian filter.

A simplified, pseudocode implementation can be expressed as follows:

```
N = 10000
STEP = 0.0001
SIGMA = 10

def streamline_origin_density(flow_map):
    particles = spawn_random_particles(in_texture=flow_map)

    streamlines = zeros((len(particles), N, 2))

    for i in range(N):
        particles = [
            apply_boundary_conditions(particle - flow_map[particle] * STEP)
            for particle in particles
        ]
        streamlines[:, i] = particles

    converged_particles = converged_streamlines(streamlines)[:, -1]

    texture = zeros(flow_map.shape[:-1])
```

```
    for particle in converged_particles:
        texture[particle] += 1

    return gaussian_filter(texture, sigma=SIGMA)
```

Examples

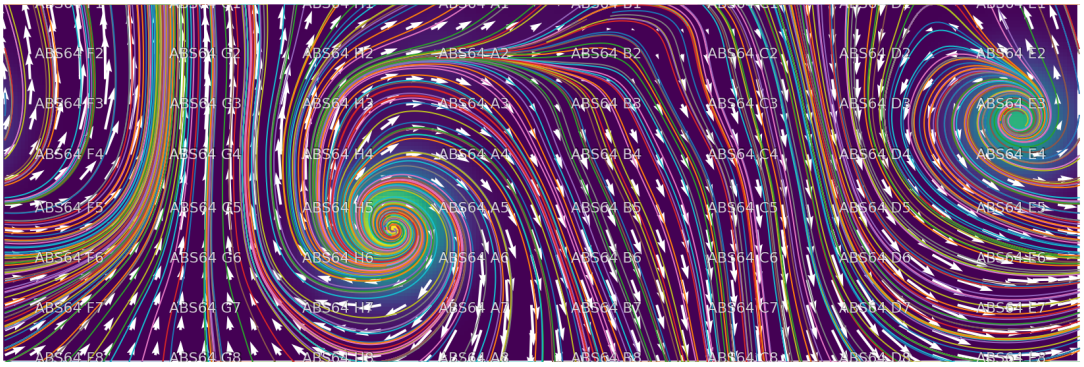

Figure 4.12: An example of a streamline origins density map, representative of 2 seconds of flow, of a patient in dataset **A**. Simulated streamlines, flow vectors and electrode labels are superimposed.

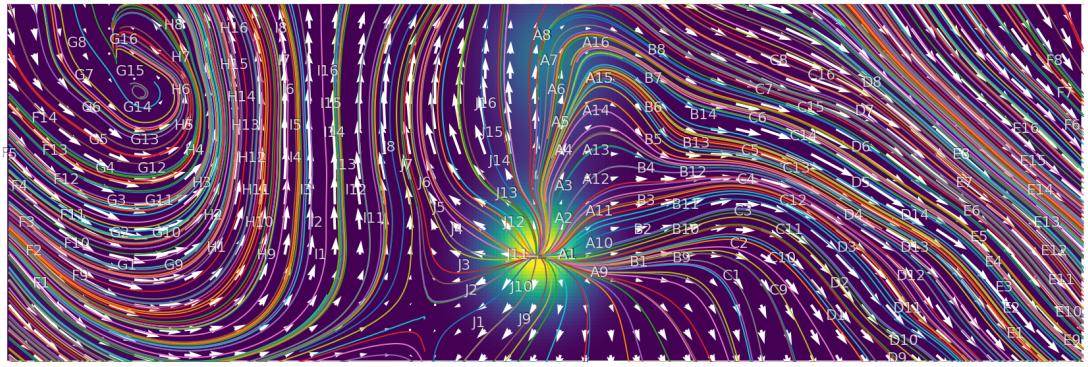

Figure 4.13: An example of a streamline origins density map, representative of 2 seconds of flow, of a patient in dataset **B**. Simulated streamlines, flow vectors and electrode labels are superimposed.

4.3.3 Sources

Purpose

To locate origins of wavefronts by quantifying divergent singularities.

Background

In the intracardiac problem space, sources have been shown to produce divergent flow patterns. Logically, this can be explained by drivers generating wave fronts that propagate outward. Divergence can be measured in several ways. One way is to locate singularities of directions in the vector field. Because of the smoothing term of the Horn& Schunck algorithm, these are unlikely to occur unless the flow is either convergent, divergent, or rotating around these singularities. Singularity analysis can further distinguish these types, which has previously been used to locate drivers using intracardiac catheter electrodes.

Computation

Source maps are computed using an algorithm developed at Ablacon, Inc. Briefly, the algorithm locates divergent singularities by convolution of flow vectors with orthogonal angles.

Examples

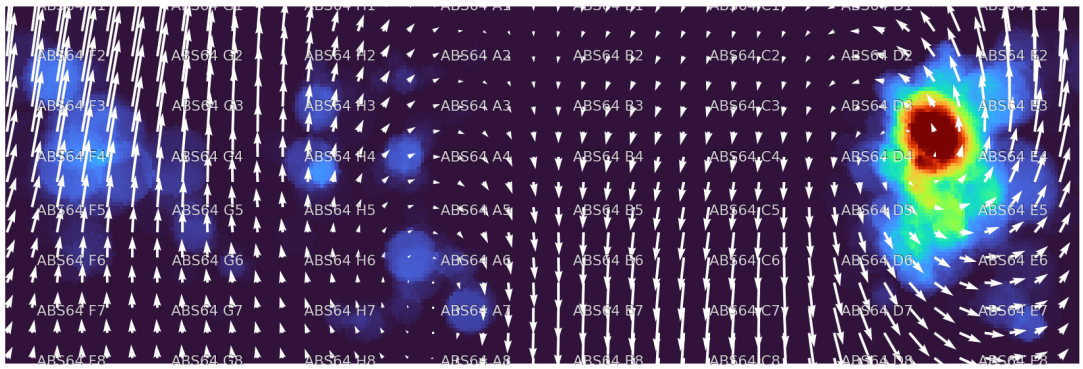

Figure 4.14: An aggregation of a source map, representative of 60 seconds of flow, of a patient in dataset **A**. The euclidean mean of flow vectors and electrode labels are superimposed.

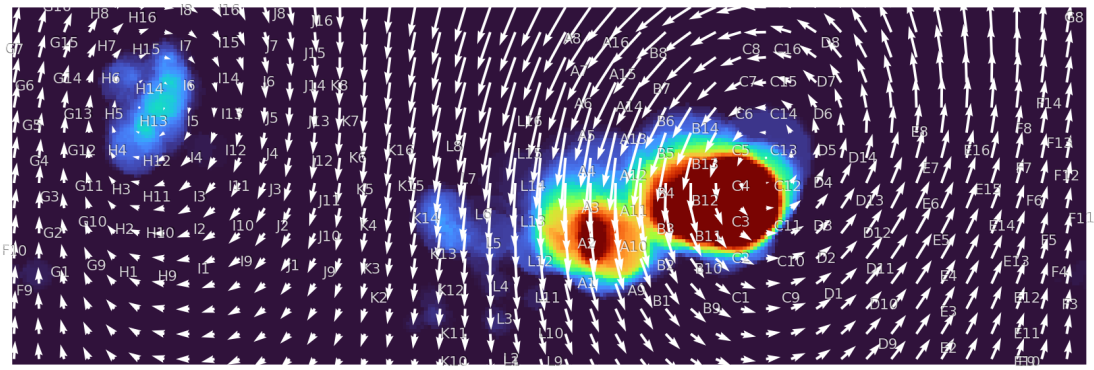

Figure 4.15: An aggregation of a source map, representative of 60 seconds of flow, of a patient in dataset **B**. The euclidean mean of flow vectors and electrode labels are superimposed.

5 Discussion

In the following chapter, the methods introduced in the previous chapters are applied to the datasets **A** and **B**. The resulting EGF maps (flow angle stability, streamline origins density, sources) are examined and observations are discussed.

Three different modalities are considered for evaluation of the methods:

1. section 5.1: Discriminability between individual patients in atrial fibrillation
2. section 5.2: Discriminability between patients in sinus rhythm and patients in atrial fibrillation
3. section 5.3: Discriminability between atrial fibrillation patients with recurrence and those without

5.1 EGF Fingerprinting: Discriminability of Flow Maps

To estimate patient discriminability, I use cross-correlation as a measure of self-similarity. Segments of flow frames are created from disjunct data from each patient and subsequently used to independently generate the corresponding feature maps. These are cross-correlated with other feature maps from the same and other patients. A similarity matrix is generated from the mean pixel-wise correlation, from which a mean correlation value for the same patient and different patient pairs can finally be calculated. A large difference between these two values is desired.

While the recordings are divided into 60-second segments for atrial isolation, 2-second segments are used for flow calculation, with an additional 2 seconds used for flow initialization. Normally, these segments use the previous segment's data for flow initialization. To avoid initializing a flow field with data from another, which could distort cross-correlations, every second segment is skipped so that there is no overlap. The resulting feature maps can be re-aggregated using pixel-wise means to test for temporal stability.

In the following tables, results are shown. Variables are named like map-type$^{dataset}_{metric}$, where map-type indicates the name of the feature map, *dataset* indicates dataset **A** or **B**, and *metric* indicates same patient or different patient similiarities, or the ratio thereof.

	Dataset **A**	Dataset **B**
2s Aggregations		
Same Patient	$\text{fas}^a_{same} = 3.32\text{e}{+04}$	$\text{fas}^b_{same} = 2.08\text{e}{+04}$
Different Patient	$\text{fas}^a_{same} = 2.35\text{e}{+04}$	$\text{fas}^b_{other} = 1.53\text{e}{+04}$
Ratio	$\text{fas}^a_{ratio} = 1.41$	$\text{fas}^b_{ratio} = 1.36$
10s Aggregations		
Same Patient	$\text{fas}^a_{same} = 3.21\text{e}{+04}$	$\text{fas}^b_{same} = 2.04\text{e}{+04}$
Different Patient	$\text{fas}^a_{same} = 2.34\text{e}{+04}$	$\text{fas}^b_{other} = 1.51\text{e}{+04}$
Ratio	$\text{fas}^a_{ratio} = 1.37$	$\text{fas}^b_{ratio} = 1.35$
60s Aggregations		
Same Patient	$\text{fas}^a_{same} = 3.04\text{e}{+04}$	$\text{fas}^b_{same} = 2.19\text{e}{+04}$
Different Patient	$\text{fas}^a_{same} = 2.31\text{e}{+04}$	$\text{fas}^b_{other} = 1.59\text{e}{+04}$
Ratio	$\text{fas}^a_{ratio} = 1.32$	$\text{fas}^b_{ratio} = 1.38$

Table 5.1: Discriminability of flow angle stability (FAS) maps between patients. Each entry represents a mean cross-correlation either between recordings of the same patient, or recordings of different patients.

	Dataset **A**	Dataset **B**
2s Aggregations		
Same Patient	$\text{sod}^a_{same} = 4.23\text{e}{-10}$	$\text{sod}^b_{same} = 4.87\text{e}{-10}$
Different Patient	$\text{sod}^a_{other} = 2.86\text{e}{-10}$	$\text{sod}^b_{other} = 2.97\text{e}{-10}$
Ratio	$\text{sod}^a_{ratio} = 1.48$	$\text{sod}^b_{ratio} = 1.64$
10s Aggregations		
Same Patient	$\text{sod}^a_{same} = 4.31\text{e}{-10}$	$\text{sod}^b_{same} = 4.94\text{e}{-10}$
Different Patient	$\text{sod}^a_{other} = 2.91\text{e}{-10}$	$\text{sod}^b_{other} = 3.02\text{e}{-10}$
Ratio	$\text{sod}^a_{ratio} = 1.48$	$\text{sod}^b_{ratio} = 1.64$
60s Aggregations		
Same Patient	$\text{sod}^a_{same} = 4.25\text{e}{-10}$	$\text{sod}^b_{same} = 4.87\text{e}{-10}$
Different Patient	$\text{sod}^a_{other} = 2.94\text{e}{-10}$	$\text{sod}^b_{other} = 3.00\text{e}{-10}$
Ratio	$\text{sod}^a_{ratio} = 1.45$	$\text{sod}^b_{ratio} = 1.63$

Table 5.2: Discriminability of streamline origins density (SOD) maps between patients. Each entry represents a mean cross-correlation either between recordings of the same patient, or recordings of different patients.

	Dataset **A**	Dataset **B**
2s Aggregations		
Same Patient	$\text{sources}^{a}_{same} = 3.72\text{e}{-05}$	$\text{sources}^{b}_{same} = 6.65\text{e}{-05}$
Different Patient	$\text{sources}^{a}_{other} = 9.88\text{e}{-06}$	$\text{sources}^{b}_{other} = 3.05\text{e}{-05}$
Ratio	$\text{sources}^{a}_{ratio} = 3.76$	$\text{sources}^{b}_{ratio} = 2.18$
10s Aggregations		
Same Patient	$\text{sources}^{a}_{same} = 3.36\text{e}{-05}$	$\text{sources}^{b}_{same} = 6.77\text{e}{-05}$
Different Patient	$\text{sources}^{a}_{other} = 9.99\text{e}{-06}$	$\text{sources}^{b}_{other} = 3.12\text{e}{-05}$
Ratio	$\text{sources}^{a}_{ratio} = 3.36$	$\text{sources}^{b}_{ratio} = 2.17$
60s Aggregations		
Same Patient	$\text{sources}^{a}_{same} = 2.96\text{e}{-05}$	$\text{sources}^{b}_{same} = 7.02\text{e}{-05}$
Different Patient	$\text{sources}^{a}_{other} = 1.05\text{e}{-05}$	$\text{sources}^{b}_{other} = 3.19\text{e}{-05}$
Ratio	$\text{sources}^{a}_{ratio} = 2.82$	$\text{sources}^{b}_{ratio} = 2.20$

Table 5.3: Discriminability of source maps between patients. Each entry represents a mean cross-correlation either between recordings of the same patient, or recordings of different patients.

5.1.1 Observations

Metrics were tested for both datasets using 2-second, 10-second, and 30-second aggregations. The results are shown in Table 5.1, Table 5.2 and Table 5.3.

All calculated ratios of similarity between same patient and different patient pairs means were significantly above 1, indicating that patient-specific information is contained in at least a subset of the feature maps. The ratios were highest for source maps ($\max(\text{sources}^{a}_{ratio}) = 3.76$), suggesting that this type of map may be best suited for ECG estimated from body surface electrodes.

Aggregation of multiple maps using means did not result in better cross-correlation ratios between same patient pairs and different patient pairs for all 3 flow maps tested. This suggests that data do not need to be aggregated for longer than 2 seconds. One possible improvement in discriminative ability that has not been tested is the use of a subset of segments to calculate the metrics. Because drivers are transient, some segments may not contain information about drivers that are critical for maintaining AFib.

5.2 Patterns of the Sinoatrial Node

To understand and test EGF maps on the body surface, a test using patients in sinus rhythm is useful. These patients have only one active pacemaker: the SA node. When mapping EGF and looking for sources, I hypothesized that exactly one source should be visible.

In contrast to AFib patients, there is an AV association in patients in SR. In other words, in these patients, the atria are active only just before ventricular contraction. Since the QRS cancellation algorithm cancels all signals that are synchronised with the R peaks, this step of atrial isolation must be adjusted to account for this fact. To achieve this, I added a time range before each R peak that is not cancelled along the ventricular component (Figure 5.1).

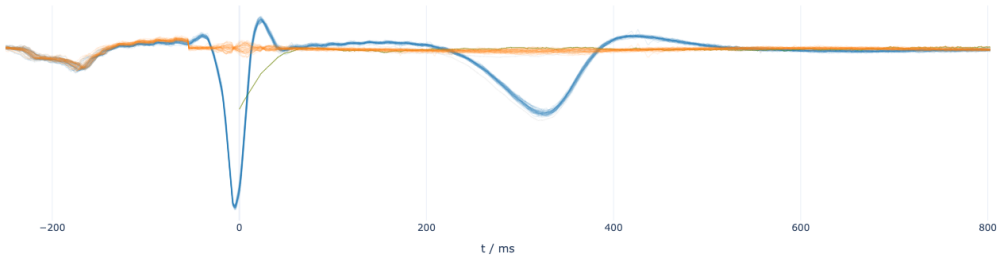

Figure 5.1: Preservation of the p-wave in a patient in sinus rhythm. The blue line shows the superimposed P-QRS-T complexes before cancellation, and the orange line shows the same time ranges after cancellation.

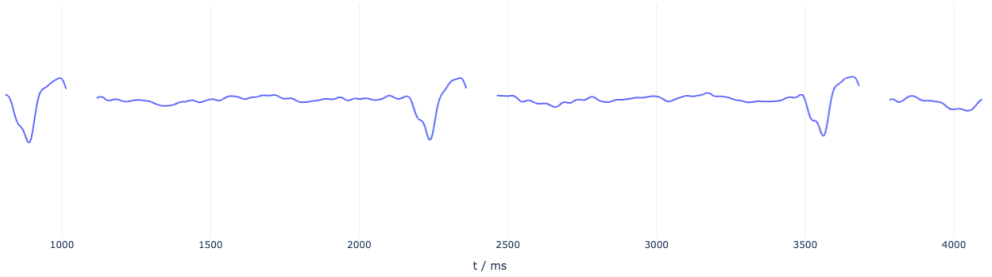

Figure 5.2: Atrial Signal Isolation in sinus rhythm patients. The graph shows an example electrode after the adjusted atrial signal isolation algorithm was applied.

After atrial isolation, the resulting signal is mostly a flat line, with the exception of the preserved P waves (Figure 5.2. In other sections, some noise remains that cannot be

readily attributed to a single component.

As an adjunct to the dataset **A**, seven recordings were acquired from healthy patients. I used these recordings to create EGF maps to test the hypothesis. Two example maps are shown here (Figure 5.3 and Figure 5.4).

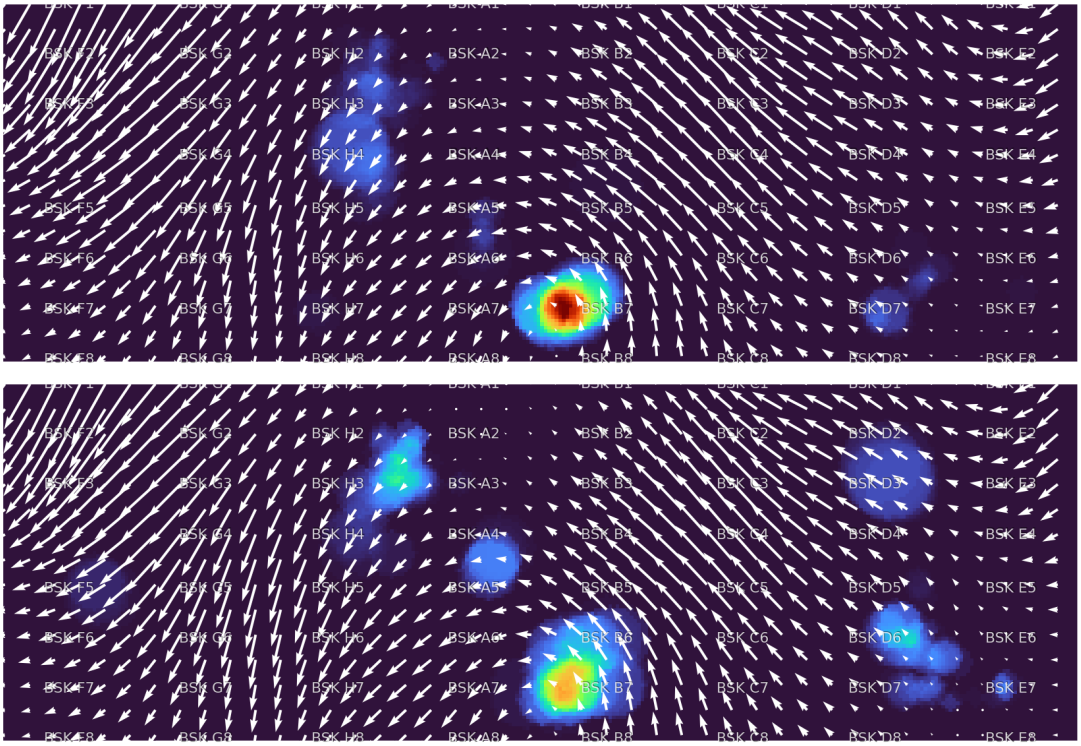

Figure 5.3: (1) 1-minute aggregated source maps of the same patient during SR. In both maps, one source can be observed.

In both examples, a source can be observed between electrodes A7 and B7 in multiple independently processed recordings. These positions correspond to the patient's lower right back.

In addition, in the second patient (Figure 5.4), a second source can be observed between electrodes E2 and E3. These positions correspond to the upper left front of the patient. Given that this position is opposite of the first when tracing a vector through the position of the atrium, the projection of atrial activity results in similar, yet mirrored traces. I hypothesize that both observed sources are the same inside the atrium, observed from two opposite angles.

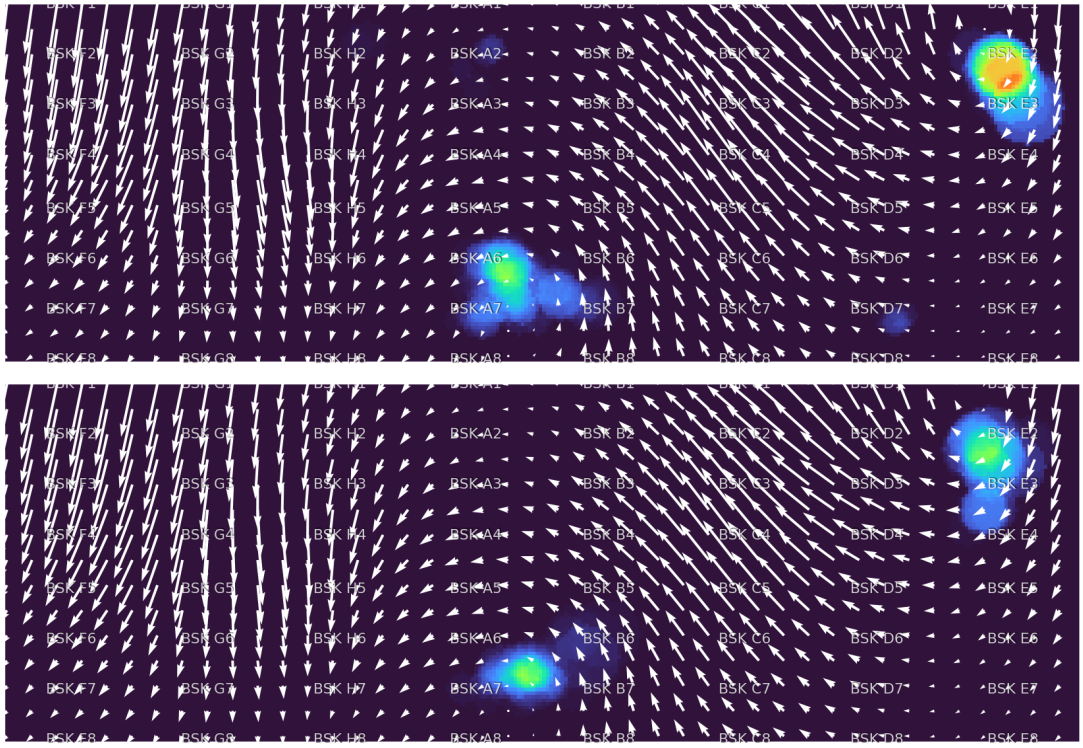

Figure 5.4: (2) 1-minute aggregated source maps of the same patient during SR. In both maps, two sources can be observed.

In all of the 7 patients, sources in either of these two locations can be observde. However, this is not true for all recordings of the patients. In particular, in some patients, these sources can be observed in nearly all recrodings, while for others, highly variable EGF maps are produced. I attribute this observation to potential sources of noise in the remainder of the signal, and postulate it should be possible to further optimize components of the pipeline, or hyperparameters thereof, to generate more consistent EGF maps. An example of a test which was not performed in this thesis is only considering the time ranges of p-waves for analysis, rather than using ventricular cancellation to negate its potential effects on the resulting flow maps.

To quantify discriminability of AFib versus SR patients, I performed cross-correlation analyses similar to those performed in section 5.1 (Table 5.4). I used source maps, as those previously had the highest ratio of discriminability between individual patients.

Some modifications to the method need to be introduced to avoid distorting the results. First, an equal number of healthy and non-healthy should be used to balance the labels. A random subselection of seven AFib patients were used. Second, flow

	Dataset **A**
2s Aggregations	
Same Patient	$\text{sources}^{ah}_{same} = 3.59\text{e}{-05}$
Different Patient	$\text{sources}^{ah}_{same} = 2.29\text{e}{-05}$
Ratio	$\text{sources}^{ah}_{ratio} = 1.56$
10s Aggregations	
Same Patient	$\text{sources}^{ah}_{same} = 3.57\text{e}{-05}$
Different Patient	$\text{sources}^{ah}_{same} = 2.29\text{e}{-05}$
Ratio	$\text{sources}^{ah}_{ratio} = 1.56$
60s Aggregations	
Same Patient	$\text{sources}^{ah}_{same} = 3.57\text{e}{-05}$
Different Patient	$\text{sources}^{ah}_{same} = 2.22\text{e}{-05}$
Ratio	$\text{sources}^{ah}_{ratio} = 1.61$

Table 5.4: Discriminability of sinus rhythm patients using source maps.

maps were only compared for different patients of the same rhythm. Otherwise, results might be distorted by the fact that same-patient feature maps may be self-similar. sources_{same} therefore indicates mean cross-correlations between different patients of the same rhythm, and sources_{other} indicates mean cross-correlations between different patients of different rhythms.

The variable sources_{same} did not change significantly when multiple segments are aggregated using means. This indicates that feature maps need not be aggregated to discriminate between patient rhythms. Another important observation is that sources_{ratio} is significantly higher for same patient cross-correlations (as shown in section 5.1) than for same rhythm cross-correlations ($\max(\text{sources}^{a}_{ratio}) = 3.76$ vs $\max(\text{sources}^{ah}_{ratio}) = 1.61$). This suggests that feature maps are more self-similar for recordings of the same patient than recordings of different patients in the same rhythm.

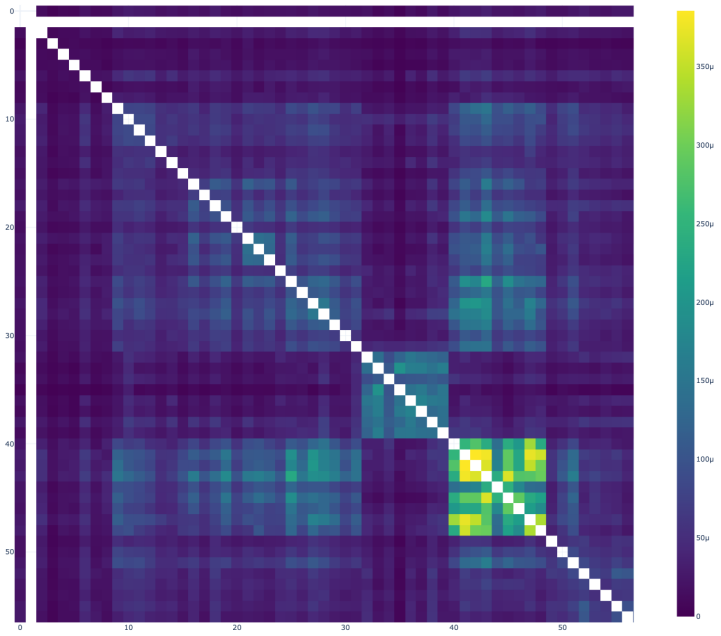

Figure 5.5: Distance matrix for source maps for patients in sinus rhythm, created using 60 second aggregations. The diagonal is colorless because they indicate cross-correlations between a source map and itself.

The distance matrix created for healthy patients (Figure 5.5) shows the cross-correlation similarity between nine source maps for each healthy patient. It can be observed that most of the source maps show increased correlation with other source maps generated from the same patient. The maps of four patients also correlate with each other. Maps of one patient correlate only with other maps of the same patient, while most maps of two other patients do not correlate significantly with any other source maps.

5.3 Correlation to Outcome

The primary endpoint considered in this thesis is spontaneous termination of AFib during ablation. This information was available in Dataset **B**. I hypothesized that if AFib drivers critical for maintaining AFib were located in the atria, a PVI would not isolate the sources and thus terminate AFib. However, if focal impulses were located in the PVs, a PVI would isolate them, and AFib would terminate.

I additionally hypothesized that sources located in the atria would be visible from

body surface EGF maps. These maps were designed based on expert knowledge and findings of previous research. To test predictiveness, feature maps were aggregated using *maximum* or *mean*. Metrics of multiple recordings of the same patient were aggregated using mean. The predictive power was then tested using point-biserial correlation r_{pb} and AUC calculated from false positive and true positive rates.

The best predictors for spontaneous termination were streamline origin density mean ($r_{pb} = 0.54$, AUC $= 0.80$), flow angle stability mean ($r_{pb} = 0.46$, AUC $= 0.82$) and source map maximum ($r_{pb} = 0.45$, AUC $= 0.78$). A graph of all 3 metrics is shown in Figure 5.6.

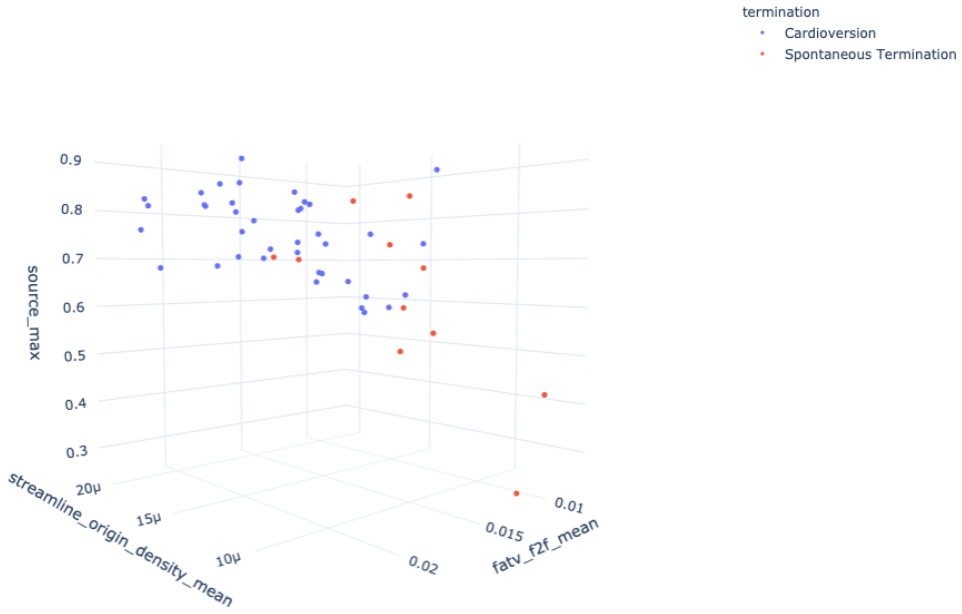

Figure 5.6: The 3 best predictors of spontaneous termination of atrial fibrillation created from aggregations of flow maps.

In addition to metrics collected from EGF maps, I collected metrics defined in previous papers and calculated them on isolated atrial component leads. The same signal was used that was also used to calculate EGF maps. Tested metrics were F-Wave magnitude mean [Nau+09], Nondipolar Component Index (NDI) [Meo+18], hjorth parameters [Hjo70], dominant frequency, organization index [Lan+16] and RQA parameters.

The 3 best predictors for spontaneous termination were organization index ($r_{pb} = 0.37$, AUC $= 0.77$), RQA vertical entropy ($r_{pb} = 0.35$, AUC $= 0.70$) and F-Wave magnitude mean ($r_{pb} = -0.30$, AUC $= 0.67$). A graph of all 3 metrics is shown in Figure 5.7.

The collected EGF metrics therefore outperform previously proposed single-lead ECG metrics.

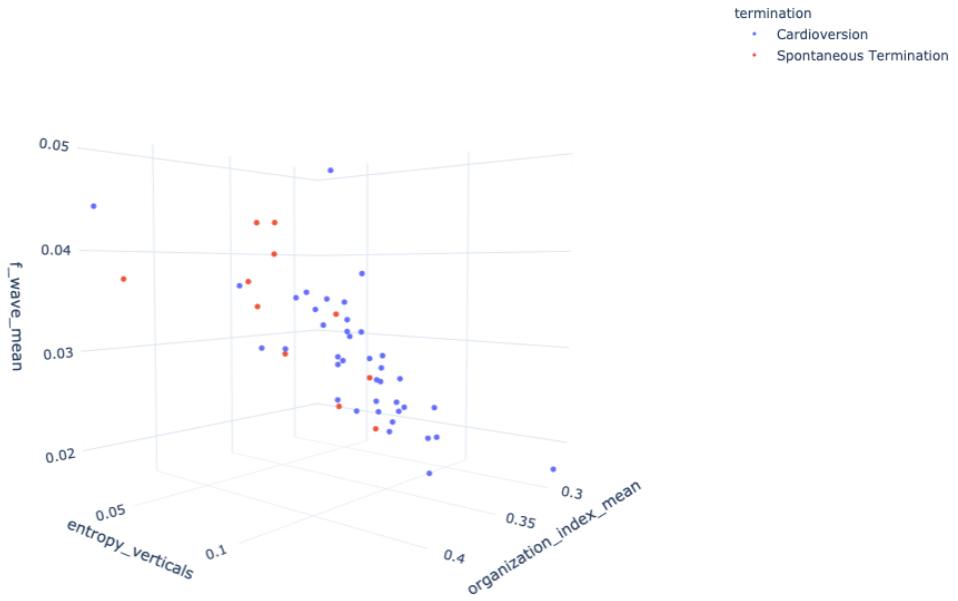

Figure 5.7: The 3 best predictors of spontaneous termination of atrial fibrillation from single-lead ECG metrics.

Another desirable quality of metrics collected prior to ablation is correlation to long-term recurrence. In both datasets, 12-month recurrence labels were available. I hypothesized that if drivers critical to maintaining AFib were located in the atria, a PVI would not suffice as treatment, and the AFib should recur.

The predictive power of metrics for 12-month recurrence was also tested using point-biserial correlation r_{pb}.

The three best EGF-based predictors for dataset **A** were source mean ($r_{pb} = 0.34$, AUC $= 0.67$), FAS mean ($r_{pb} = 0.32$, AUC $= 0.65$) and SOD mean ($r_{pb} = 0.24$, AUC $= 0.56$). The three best EGF-based predictors for dataset **B** were streamline origin density mean ($r_{pb} = 0.22$, AUC $= 0.59$), source map mean ($r_{pb} = 0.21$, AUC $= 0.59$), and flow angle stability mean ($r_{pb} = 0.18$, AUC $= 0.60$). Graphs of all best predictors are shown in Figure 5.8.

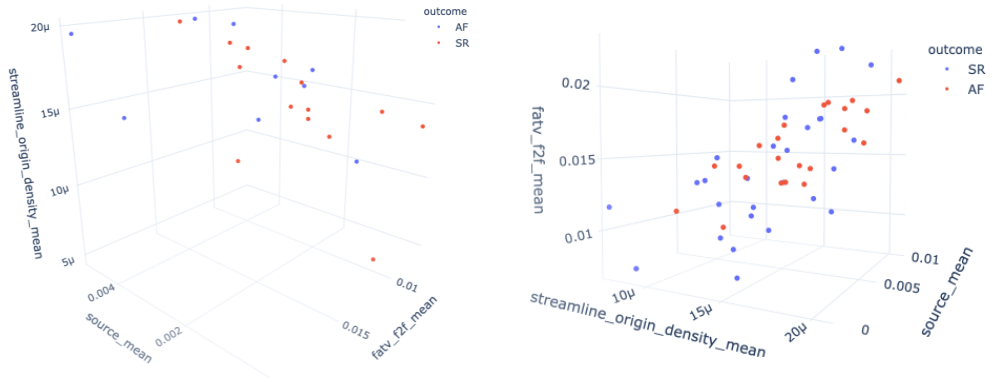

Figure 5.8: The 3 best predictors of recurrence created from aggregations of flow maps for the datasets **A** (left) and **B** (right).

I also compared the recurrence predictors with the previously proposed single-lead ECG metrics to test predictive performance. The top three predictors in dataset **A** were dominant frequency ($r_{pb} = 0.23$, AUC $= 0.62$), diagonal entropy ($r_{pb} = -0.23$, AUC $= 0.67$) and RQA determinism ($r_{pb} = -0.19$, AUC $= 0.74$). The three best predictors in dataset **B** were F-Wave magnitude mean ($r_{pb} = -0.48$, AUC $= 0.77$), RQA vertical entropy ($r_{pb} = 0.42$, AUC $= 0.71$) and RQA recurrence ($r_{pb} = 0.41$, AUC $= 0.74$). Graphs of all best predictors are shown in Figure 5.9.

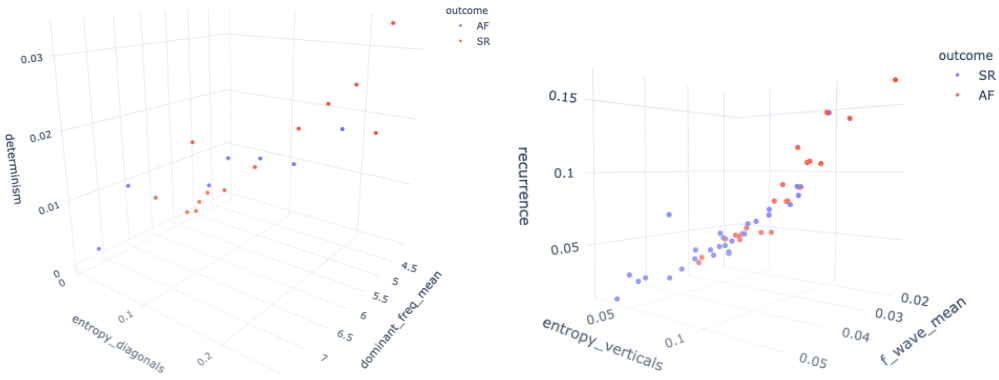

Figure 5.9: The 3 best predictors of recurrence from single-lead ECG metrics for the datasets **A** (left) and **B** (right).

6 Conclusion

In this thesis, I tested the hypothesis of whether drivers of atrial fibrillation can be mapped from dense body surface electrodes using electrographic flow. To achieve this, I introduced a pipeline capable of separating atrial signals and then used the separated atrial component to generate three types of EGF maps. I tested the performance of the pipeline using several methods: First, the discriminability between patients. Second, discriminability between heart rhythms. Third, predictiveness for spontaneous conversion during subsequent ablations. Fourth, the preditiveness for long-term recurrence of atrial fibrillation after a PVI.

The calculated feature maps all showed significant discriminability between patients, with source maps for 2-second flow maps in dataset **A** performing best ($\text{sources}^{a}_{ratio} = 3.76$).

Self-similarity of patients with SR versus patients with AFib was also demonstrated. Here, the best-performing cross-correlation similarity metric were 2-second source maps ($\text{sources}^{ah}_{ratio} = 1.61$).

Metrics created from aggregates of all three types of flow maps were able to outperform previously proposed single-lead ECG metrics for the prediction of spontaneous termination of AFib during ablation. The best performing metric, flow angle stability mean, achieved an AUC of 0.82. I conclude that EGF is well suited for this task.

Results for prediction of recurrence were inconclusive. EGF-based metrics were able to outperform the previously proposed parameters in the smaller dataset **A**. However, they were outperformed in the larger dataset **B**. I conclude that a larger-scale study with more rigorous monitoring or different endpoints may be needed. However, there are many factors that could lead to a recurrence or lack thereof. It is possible that EGF-based metrics may complement previously proposed single-lead metrics.

I conclude that EGF is suitable for mapping atrial fibrillation on the body surface. This eliminates the need for expensive and invasive CT scans to perform inverse projections. Hopefully, with future optimizations, this method can be perfected and used to guide treatment, ablation, or risk assessment.

6.1 Future Work

The conclusions drawn from this thesis are limited in several ways.

First, the algorithm for isolating atrial signals consists of many techniques, some of which are already proven, while others were presented for the first time in this thesis. For each, one could define quantification analyses and perform more in-depth hyperparameter optimization. However, ground truth knowledge of perfect separation is difficult to define. Simple superimposition of generated signals is arbitrary and may not represent real-world data. Another option is to use simulated data using software such as OpenCARP.

Second, the data set for healthy patient recordings was limited in number of patients, and therefore conclusions drawn from it may not be generalizable. A larger dataset could be collected and a more detailed analysis could be performed. It may be possible to derive additional information from these data, such as the presence of low voltage areas. This information could serve as a measure of the risk of developing atrial fibrillation, as previous studies have shown their role in maintaining AFib [McG+14; Lau+17; Pla17; Sah+18; Nad+04].

Third, the recurrence labels did not adhere to the standards recommended in an expert consensus [Cal+17]. In addition, the labels are not interchangeable with the presence of intracardiac arrhythmia drivers. A modality other than recurrence could be used as ground truth to meaningfully predict this fact. One possible modality would be the recording of body surface electrodes during an invasive intervention. Possible labels could be based on intracardiac electrodes or whether a PVI terminates AFib.

Finally, future studies could improve the cost-effectiveness of the analysis. Dataset **A** used 64 electrodes and Dataset **B** used 240. It is not clear whether 240 electrodes are required. In addition, it could be investigated whether a subset of these on smaller areas of the torso would be sufficient. Reduced time and resources could significantly improve adaptability in clinical settings.

Appendices

.1 A Complete Example of Atrial Signal Isolation

Here, a complete example of the atrial isolation algorithm is presented. The all-channel average subtraction step is omitted because the used amplifier (TMSi Refa) performs an all-channel average subtraction as part of the recording process.

Processing steps are provided as images of voltages over time. The x-axis represents time, in seconds, to a total of 4 plotted seconds. The y-axis represents individual electrodes. The values, in millivolt, are shown in the colormap for each image.

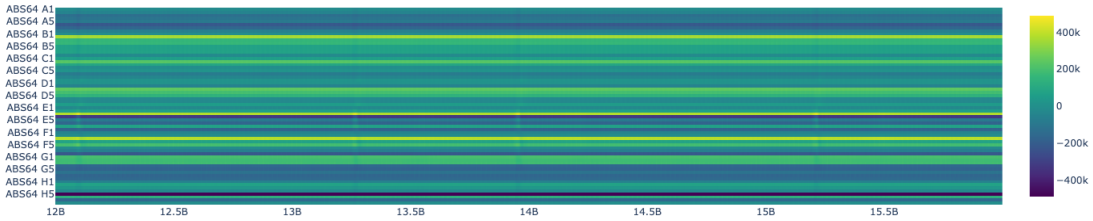

Figure .1: Input Signal

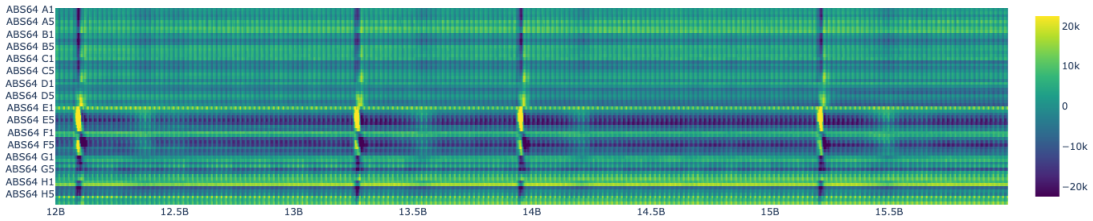

Figure .2: Zero-Centering

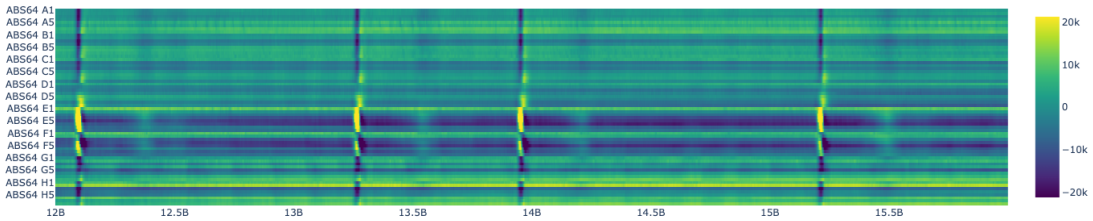

Figure .3: Mains Hum Correction

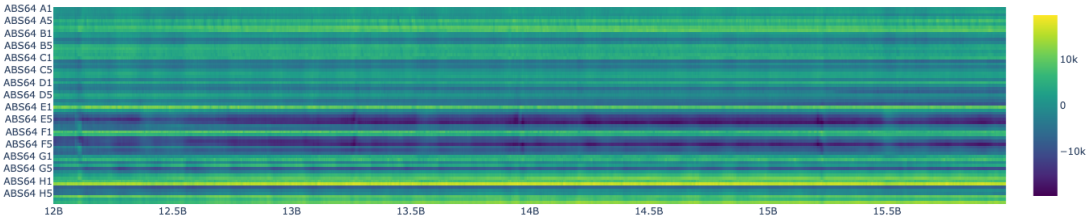

Figure .4: Ventricular Cancellation

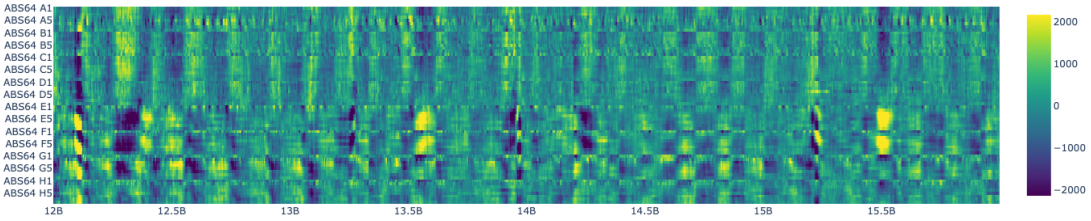

Figure .5: Baseline Wander Correction

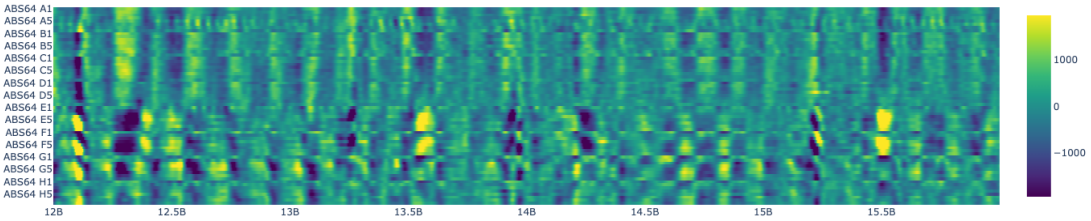

Figure .6: Lowpass

Glossary

Antiarrhythmic Drug (AAD) AADs are a group of pharmaceuticals that are used to suppress abnormal rhythms of the heart. . 1, 2, 8

Atrial Fibrillation (AFib) is a disorder of the heart that produces irregular, often rapid heartbeats without an apparent pattern. . 1, 2, 4–11, 13–15, 22, 29, 31, 40, 41, 43, 45, 47, 49, 50, 55

AUC Area under Curve. 9, 46–49

AV Atrioventricular. 2, 22, 41, 55

BS Body Surface. 3, 13

CA Catheter Ablation. 1, 2, 7, 8

CT Computed Tomography. 10, 49

DWT Discrete Wavelet Transformation. 21

Electrocardiagram (ECG) is timeseries data of electrical activity originating from the heart. . 2–4, 9, 10, 12–14, 17, 20, 22, 40, 47–49

ECGI Electrocardiographic Imaging. 10

Electrographic Flow (EGF) is a novel technology [Bel+18] for the identification and characterization of atrial fibrillation drivers in humans. It uses the Horn & Schunck algorithm [HS81] to estimate optical flow based on intracardiac catheter data. . 2–4, 11, 12, 31, 38, 41–43, 46, 47, 49

eGFR Estimated Glomerular Filtration Rate. 9

ESC European Society of Cardiology. 1

FAS Flow Angle Stability. 28, 32, 47

FFT Fast Fourier Transform. 20

Fibrillatory Wave (F-Wave) A fibrillatory wave is an excitation, as observed from electrodes, that originates from the atria during atrial fibrillation. P-Waves, which also originate in the atria, only exist per definition in SR patients and are synchronized to ventricular excitation. . 10, 28, 46, 48

GP Ganglionated Plexi. 8

Cardioversion (CV) is a technique for restoring SR in AFib patients.. 1

LA Left Atrial. 9

LGE-MRI Late Gadolinium Enhanced Magnetic Resonance Imaging. 9

NDI Nondipolar Component Index. 46

PCA Principal Component Analysis. 11

PV Pulmonary Vein. 2, 7, 8, 10, 11, 45

PVC Premature Ventricular Contraction. 26

Pulmonary Vein Isolation (PVI) is an invasive intervention where the pulmonary veins are electrically isolated from the atria. . 2, 3, 6–8, 13, 14, 45, 47, 49, 50

Quality of Life (QOL) : "an individual's perception of their position in life in the context of the culture and value systems in which they live and in relation to their goals, expectations, standards and concerns." (WHO). . 1, 8

RBF Radial Basis Function. 28

RQA Recurrence Quantification Analysis. 11, 46, 48

SA Sinoatrial. 1, 2, 5, 55

SOD Streamline Origin Density. 34, 47

Sinus Rhythm (SR) The common state of ventricular contractions. The SA node generates signal, which propagates through the atria to the AV node and further causes ventricular contraction. . 1, 7, 41–43, 49, 55

STD Standard Deviation. 11

List of Figures

List of Tables

Bibliography

[] *Measurement of the mains frequency, howpublished = https://www.mainsfrequency.com/, note = Accessed: 2021-01-01.*

[Bel+18] B. Bellmann, T. Lin, J. Ruppersberg, et al. "Identification of active atrial fibrillation sources and their discrimination from passive rotors using electrographical flow mapping." In: *Clinical Research in Cardiology* 107 (Nov. 2018). DOI: 10.1007/s00392-018-1274-7.

[Bel+19] B. Bellmann, M. Zettwitz, T. Lin, et al. "Velocity Characteristics of Atrial Fibrillation Sources determined by Electrographic Flow Mapping before and after Catheter Ablation." In: *International Journal of Cardiology* 286 (Feb. 2019). DOI: 10.1016/j.ijcard.2019.02.006.

[BL88] D. Broomhead and D. Lowe. "Radial basis functions, multi-variable functional interpolation and adaptive networks." In: *ROYAL SIGNALS AND RADAR ESTABLISHMENT MALVERN (UNITED KINGDOM)* RSRE-MEMO-4148 (Mar. 1988).

[Cal+17] H. Calkins, G. Hindricks, R. Cappato, et al. "2017 HRS/EHRA/ECAS/APHRS/-SOLAECE expert consensus statement on catheter and surgical ablation of atrial fibrillation." In: *EP Europace* 20.1 (Sept. 2017), e1–e160. ISSN: 1099-5129. DOI: 10.1093/europace/eux274. eprint: https://academic.oup.com/europace/article-pdf/20/1/e1/24119989/eux274.pdf.

[Cam+12] A. J. Camm, G. Lip, R. De Caterina, et al. "ESC Committee for Practice Guidelines (CPG). 2012 focused update of the ESC Guidelines for the management of atrial fibrillation: an update of the 2010 ESC Guidelines for the management of atrial fibrillation. Developed with the special contribution of the European Heart Rhythm Association." In: *Eur Heart J* 33.21 (2012), pp. 2719–2747.

[Cos+12] J. Cosedis Nielsen, A. Johannessen, P. Raatikainen, et al. "Radiofrequency Ablation as Initial Therapy in Paroxysmal Atrial Fibrillation." In: *New England Journal of Medicine* 367.17 (2012). PMID: 23094720, pp. 1587–1595. DOI: 10.1056/NEJMoa1113566. eprint: https://doi.org/10.1056/NEJMoa1113566.

[CSB00] J. L. Cox, R. B. Schuessler, and J. P. Boineau. "The Development of the Maze Procedure for the Treatment of Atrial Fibrillation." In: *Seminars in Thoracic and Cardiovascular Surgery* 12.1 (2000), pp. 2–14. ISSN: 1043-0679. DOI: https://doi.org/10.1016/S1043-0679(00)70010-4.

[Cuc+10] P. S. Cuculich, Y. Wang, B. D. Lindsay, et al. "Noninvasive Characterization of Epicardial Activation in Humans With Diverse Atrial Fibrillation Patterns." In: *Circulation* 122.14 (2010), pp. 1364–1372. DOI: 10.1161/CIRCULATIONAHA.110.945709. eprint: https://www.ahajournals.org/doi/pdf/10.1161/CIRCULATIONAHA.110.945709.

[Dre+20] J. Dretzke, N. Chuchu, R. Agarwal, et al. "Predicting recurrent atrial fibrillation after catheter ablation: A systematic review of prognostic models." In: *Europace* 22 (Mar. 2020). DOI: 10.1093/europace/euaa041.

[Est+96] M. Ester, H.-P. Kriegel, J. Sander, and X. Xu. "A Density-Based Algorithm for Discovering Clusters in Large Spatial Databases with Noise." In: *Proceedings of the Second International Conference on Knowledge Discovery and Data Mining*. KDD'96. Portland, Oregon: AAAI Press, 1996, pp. 226–231.

[Faz07] T. Fazekas. "[The concise history of atrial fibrillation]." In: *Orvostörténeti közlemények* 53 (Feb. 2007), pp. 37–68.

[Fri+03] J. Friberg, P. Buch, H. Scharling, et al. "Rising rates of hospital admissions for atrial fibrillation." In: *Epidemiology* (2003), pp. 666–672.

[Gai+08] F. Gaita, D. Caponi, M. Scaglione, et al. "Long-Term Clinical Results of 2 Different Ablation Strategies in Patients With Paroxysmal and Persistent Atrial Fibrillation." In: *Circulation. Arrhythmia and electrophysiology* 1 (Oct. 2008), pp. 269–75. DOI: 10.1161/CIRCEP.108.774885.

[Gar+18] M. Garcia, M. Martínez-Iniesta, J. Ródenas García, et al. "A novel wavelet-based filtering strategy to remove powerline interference from electrocardiograms with atrial fibrillation." In: *Physiological Measurement* 39 (Oct. 2018). DOI: 10.1088/1361-6579/aae8b1.

[GSJ15] P. Gupta, K. K. Sharma, and S. D. Joshi. "Baseline wander removal of electrocardiogram signals using multivariate empirical mode decomposition." In: *Healthcare technology letters* 2.6 (2015), pp. 164–166.

[Hai+14] M. Haissaguerre, M. Hocini, A. Denis, et al. "Driver Domains in Persistent Atrial Fibrillation." In: *Circulation* 130.7 (2014), pp. 530–538. DOI: 10.1161/CIRCULATIONAHA.113.005421. eprint: https://www.ahajournals.org/doi/pdf/10.1161/CIRCULATIONAHA.113.005421.

[Haï+98] M. Haïssaguerre, P. Jaïs, D. C. Shah, et al. "Spontaneous Initiation of Atrial Fibrillation by Ectopic Beats Originating in the Pulmonary Veins." In: *New England Journal of Medicine* 339.10 (1998). PMID: 9725923, pp. 659–666. DOI: 10.1056/NEJM199809033391003. eprint: https://doi.org/10.1056/NEJM199809033391003.

[Hjo70] B. Hjorth. "EEG analysis based on time domain properties." In: *Electroencephalography and Clinical Neurophysiology* 29.3 (1970), pp. 306–310. ISSN: 0013-4694. DOI: https://doi.org/10.1016/0013-4694(70)90143-4.

[HS81] B. Horn and B. Schunck. "Determining Optical Flow." In: *Artificial Intelligence* 17 (Aug. 1981), pp. 185–203. DOI: 10.1016/0004-3702(81)90024-2.

[Kan+98] W. Kannel, P. Wolf, E. Benjamin, and D. Levy. "Prevalence, incidence, prognosis, and predisposing conditions for atrial fibrillation: Population-based estimates." In: *American Journal of Cardiology - AMER J CARDIOL* 82 (Oct. 1998). DOI: 10.1016/S0002-9149(98)00583-9.

[KD07] A. Khawaja and O. Dössel. "Predicting the QRS complex and detecting small changes using principal component analysis." In: *Biomedizinische Technik. Biomedical engineering* 52 (Feb. 2007), pp. 11–7. DOI: 10.1515/BMT.2007.004.

[Kim+20] J. Y. Kim, Y. Kim, G.-H. Oh, et al. "A deep learning model to predict recurrence of atrial fibrillation after pulmonary vein isolation." In: *International Journal of Arrhythmia* 21 (2020), pp. 1–7.

[Kne+17] S. Knecht, M. Sohal, I. Deisenhofer, et al. "Multicentre evaluation of non-invasive biatrial mapping for persistent atrial fibrillation ablation: the AFACART study." In: *EP Europace* 19.8 (Feb. 2017), pp. 1302–1309. ISSN: 1099-5129. DOI: 10.1093/europace/euw168. eprint: https://academic.oup.com/europace/article-pdf/19/8/1302/19614080/euw168.pdf.

[KR20] P. Kowey and V. Robinson. "The Relentless Pursuit of New Drugs to Treat Cardiac Arrhythmias." In: *Circulation* 141 (May 2020), pp. 1507–1509. DOI: 10.1161/CIRCULATIONAHA.119.045149.

[Kup+09] S. Kuppahally, E. Foster, S. Shoor, and A. Steimle. "Short-term and long-term success of electrical cardioversion in atrial fibrillation in managed care system." In: *International archives of medicine* 2 (Dec. 2009), p. 39. DOI: 10.1186/1755-7682-2-39.

[Lan+16] T. Lankveld, S. Zeemering, D. Scherr, et al. "Atrial Fibrillation Complexity Parameters Derived From Surface ECGs Predict Procedural Outcome and Long-Term Follow-Up of Stepwise Catheter Ablation for Atrial Fibrillation." In: *Circulation: Arrhythmia and Electrophysiology* 9 (Feb. 2016), e003354. DOI: 10.1161/CIRCEP.115.003354.

[Lau+17] D. H. Lau, D. Linz, U. Schotten, et al. "Pathophysiology of paroxysmal and persistent atrial fibrillation: rotors, foci and fibrosis." In: *Heart, Lung and Circulation* 26.9 (2017), pp. 887–893.

[LDI21] T. Lewis, A. N. Drury, and C. C. Iliescu. "Further observations upon the state of rapidfire-excitation of the auricles." In: *Heart* 8 (1921), pp. 311–340.

[Lei+18] M. Lei, L. Wu, D. A. Terrar, and C. L.-H. Huang. "Modernized Classification of Cardiac Antiarrhythmic Drugs." In: *Circulation* 138.17 (2018), pp. 1879–1896. DOI: 10.1161/CIRCULATIONAHA.118.035455. eprint: https://www.ahajournals.org/doi/pdf/10.1161/CIRCULATIONAHA.118.035455.

[Luo+20] G. Luongo, L. Azzolin, M. Rivolta, et al. "Non-Invasive Identification of Atrial Fibrillation Driver Location Using the 12-lead ECG: Pulmonary Vein Rotors vs. other Locations." In: vol. 2020. Aug. 2020. DOI: 10.1109/EMBC44109.2020.9176135.

[Man+18] I. Mann, B. Sandler, N. Linton, and P. Kanagaratnam. "Drivers of Atrial Fibrillation: Theoretical Considerations and Practical Concerns." In: *Arrhythmia & electrophysiology review* 7 1 (2018), pp. 49–54.

[Mar+18] N. F. Marrouche, J. Brachmann, D. Andresen, et al. "Catheter Ablation for Atrial Fibrillation with Heart Failure." In: *New England Journal of Medicine* 378.5 (2018). PMID: 29385358, pp. 417–427. DOI: 10.1056/NEJMoa1707855. eprint: https://doi.org/10.1056/NEJMoa1707855.

[Mar+19] D. Mark, K. Anstrom, S. Sheng, et al. "Effect of Catheter Ablation vs Medical Therapy on Quality of Life Among Patients With Atrial Fibrillation: The CABANA Randomized Clinical Trial." In: *JAMA* 321 (Mar. 2019). DOI: 10.1001/jama.2019.0692.

[McG+14] C. McGann, N. Akoum, A. Patel, et al. "Atrial fibrillation ablation outcome is predicted by left atrial remodeling on MRI." In: *Circulation: Arrhythmia and Electrophysiology* 7.1 (2014), pp. 23–30.

[MD+19] D. M.D, D. Mark, R. Robb, et al. "Effect of Catheter Ablation vs Antiarrhythmic Drug Therapy on Mortality, Stroke, Bleeding, and Cardiac Arrest Among Patients With Atrial Fibrillation: The CABANA Randomized Clinical Trial." In: *JAMA* 321 (Mar. 2019). DOI: 10.1001/jama.2019.0693.

[Meo+15] M. Meo, A. R. Hidalgo-Muñoz, V. Zarzoso, et al. "F-wave amplitude stability on multiple electrocardiogram leads in atrial fibrillation." In: *2015 Computing in Cardiology Conference (CinC)*. 2015, pp. 505–508. DOI: 10.1109/CIC.2015.7410958.

[Meo+18] M. Meo, T. Pambrun, N. Derval, et al. "Noninvasive Assessment of Atrial Fibrillation Complexity in Relation to Ablation Characteristics and Outcome." In: *Frontiers in Physiology* 9 (2018), p. 929. ISSN: 1664-042X. DOI: 10.3389/fphys.2018.00929.

[Mor+14] C. A. Morillo, A. Verma, S. J. Connolly, et al. "Radiofrequency Ablation vs Antiarrhythmic Drugs as First-Line Treatment of Paroxysmal Atrial Fibrillation (RAAFT-2): A Randomized Trial." In: *JAMA* 311.7 (Feb. 2014), pp. 692–700. ISSN: 0098-7484. DOI: 10.1001/jama.2014.467. eprint: https://jamanetwork.com/journals/jama/articlepdf/1829990/joi140008.pdf.

[Nad+04] K. Nademanee, J. McKenzie, E. Kosar, et al. "A new approach for catheter ablation of atrial fibrillation: mapping of the electrophysiologic substrate." In: *Journal of the American College of Cardiology* 43.11 (2004), pp. 2044–2053. ISSN: 0735-1097. DOI: https://doi.org/10.1016/j.jacc.2003.12.054.

[Nak+19] Y. Nakatani, T. Sakamoto, Y. Yamaguchi, et al. "P-wave vector magnitude predicts the left atrial low-voltage area in patients with paroxysmal atrial fibrillation." In: *Journal of Electrocardiology* 59 (Dec. 2019). DOI: 10.1016/j.jelectrocard.2019.12.015.

[Nau+09] I. Nault, N. Lellouche, S. Matsuo, et al. "Clinical value of fibrillatory wave amplitude on surface ECG in patients with persistent atrial fibrillation." In: *Journal of interventional cardiac electrophysiology : an international journal of arrhythmias and pacing* 26.1 (Oct. 2009), pp. 11–19. ISSN: 1383-875X. DOI: 10.1007/s10840-009-9398-3.

[Ner+16] P. B. Nery, D. Belliveau, G. M. Nair, et al. "Relationship Between Pulmonary Vein Reconnection and Atrial Fibrillation Recurrence: A Systematic Review and Meta-Analysis." In: *JACC: Clinical Electrophysiology* 2.4 (2016), pp. 474–483. DOI: 10.1016/j.jacep.2016.02.003. eprint: https://www.jacc.org/doi/pdf/10.1016/j.jacep.2016.02.003.

[Oos03] A. v. Oosterom. "Source models in inverse electrocardiography." In: (2003).

[Oos12] A. Oosterom. "The inverse problem of bioelectricity: An evaluation." In: *Medical & biological engineering & computing* 50 (July 2012), pp. 891–902. DOI: 10.1007/s11517-012-0941-5.

[Pac+13] D. L. Packer, R. C. Kowal, K. R. Wheelan, et al. "Cryoballoon Ablation of Pulmonary Veins for Paroxysmal Atrial Fibrillation: First Results of the North American Arctic Front (STOP AF) Pivotal Trial." In: *Journal of the American College of Cardiology* 61.16 (2013), pp. 1713–1723. ISSN: 0735-1097. DOI: https://doi.org/10.1016/j.jacc.2012.11.064.

[Pad+17] G. Padfield, C. Steinberg, J. Swampillai, et al. "Progression of Paroxysmal to Persistent Atrial Fibrillation: Canadian Registry of Atrial Fibrillation 10-Year Follow Up." In: *Heart rhythm* 14 (Feb. 2017). DOI: 10.1016/j.hrthm.2017.01.038.

[Pla17] P. G. Platonov. "Atrial fibrosis: an obligatory component of arrhythmia mechanisms in atrial fibrillation?" In: *Journal of geriatric cardiology: JGC* 14.4 (2017), p. 233.

[PNJ09] S. S. PO, H. NAKAGAWA, and W. M. JACKMAN. "Localization of Left Atrial Ganglionated Plexi in Patients with Atrial Fibrillation." In: *Journal of Cardiovascular Electrophysiology* 20.10 (2009), pp. 1186–1189. DOI: https://doi.org/10.1111/j.1540-8167.2009.01515.x. eprint: https://onlinelibrary.wiley.com/doi/pdf/10.1111/j.1540-8167.2009.01515.x.

[Ram+04] C. Ramanathan, R. N. Ghanem, P. Jia, et al. "Noninvasive electrocardiographic imaging for cardiac electrophysiology and arrhythmia." In: *Nature medicine* 10.4 (2004), pp. 422–428.

[Rua+18] C. Ruaengsri, M. R. Schill, A. J. Khiabani, et al. "The Cox-maze IV procedure in its second decade: still the gold standard?" In: *European Journal of Cardio-Thoracic Surgery* 53.suppl_1 (Mar. 2018), pp. i19–i25. ISSN: 1010-7940. DOI: 10.1093/ejcts/ezx326. eprint: https://academic.oup.com/ejcts/article-pdf/53/suppl_1/i19/25085381/ezx326.pdf.

[Sah+04] J. Sahadevan, K. Ryu, L. Peltz, et al. "Epicardial Mapping of Chronic Atrial Fibrillation in Patients." In: *Circulation* 110.21 (2004), pp. 3293–3299. DOI: 10.1161/01.CIR.0000147781.02738.13. eprint: https://www.ahajournals.org/doi/pdf/10.1161/01.CIR.0000147781.02738.13.

[Sah+18] M. Saha, C. H. Roney, J. D. Bayer, et al. "Wavelength and fibrosis affect phase singularity locations during atrial fibrillation." In: *Frontiers in physiology* 9 (2018), p. 1207.

[Sch+82] M. M. Scheinman, F. Morady, D. S. Hess, and R. Gonzalez. "Catheter-Induced Ablation of the Atrioventricular Junction to Control Refractory Supraventricular Arrhythmias." In: *JAMA* 248.7 (Aug. 1982), pp. 851–855.

ISSN: 0098-7484. DOI: 10.1001/jama.1982.03330070039027. eprint: https://jamanetwork.com/journals/jama/articlepdf/376777/jama_248_7_027.pdf.

[Sha+20] J. K. Shade, R. L. Ali, D. Basile, et al. "Preprocedure Application of Machine Learning and Mechanistic Simulations Predicts Likelihood of Paroxysmal Atrial Fibrillation Recurrence Following Pulmonary Vein Isolation." In: *Circulation: Arrhythmia and Electrophysiology* 13.7 (2020), e008213. DOI: 10.1161/CIRCEP.119.008213. eprint: https://www.ahajournals.org/doi/pdf/10.1161/CIRCEP.119.008213.

[Sin+05] B. N. Singh, S. N. Singh, D. J. Reda, et al. "Amiodarone versus Sotalol for Atrial Fibrillation." In: *New England Journal of Medicine* 352.18 (2005). PMID: 15872201, pp. 1861–1872. DOI: 10.1056/NEJMoa041705. eprint: https://doi.org/10.1056/NEJMoa041705.

[Ste+01] S. Stewart, K. MacIntyre, M. MacLeod, et al. "Trends in hospital activity, morbidity and case fatality related to atrial fibrillation in Scotland, 1986–1996." In: *European heart journal* 22.8 (2001), pp. 693–701.

[Stu+07] J. Stulak, J. Dearani, T. Sundt, et al. "Superiority of cut-And-sex technique for the Cox-maze procedure: Comparison with radiofrequency ablation." In: *The Journal of thoracic and cardiovascular surgery* 133 (May 2007), pp. 1022–7. DOI: 10.1016/j.jtcvs.2006.09.115.

[Sun+19] Z. Sun, X. Wang, X. Wang, et al. "Removal of Baseline Wander in ECG Signals Using Singular Spectrum Analysis." In: *2019 IEEE 9th International Conference on Electronics Information and Emergency Communication (ICEIEC)*. 2019, pp. 391–394. DOI: 10.1109/ICEIEC.2019.8784679.

[Swa94] J. F. Swartz. "A catheter-based curative approach to atrial fibrillation in humans." In: *Circulation* 90 (1994), pp. I–335.

[Swe+19] M. Swerdlow, M. Tamboli, M. Alhusseini, et al. "Comparing phase and electrographic flow mapping for persistent atrial fibrillation." In: *Pacing and Clinical Electrophysiology* 42.5 (2019), pp. 499–507. DOI: https://doi.org/10.1111/pace.13649. eprint: https://onlinelibrary.wiley.com/doi/pdf/10.1111/pace.13649.

[Til+20] R. R. Tilz, C. Lenz, P. Sommer, et al. "Focal Impulse and Rotor Modulation Ablation vs. Pulmonary Vein isolation for the treatment of paroxysmal Atrial Fibrillation: results from the FIRMAP AF study." In: *EP Europace* (Dec. 2020). euaa378. ISSN: 1099-5129. DOI: 10.1093/europace/euaa378. eprint: https://academic.oup.com/europace/advance-article-pdf/doi/10.1093/europace/euaa378/35060533/euaa378.pdf.

[Wan+19] X.-k. Wan, H. Wu, F. Qiao, et al. "Electrocardiogram Baseline Wander Suppression Based on the Combination of Morphological and Wavelet Transformation Based Filtering." In: *Computational and Mathematical Methods in Medicine* 2019 (Mar. 2019), pp. 1–7. DOI: 10.1155/2019/7196156.

[Wil+10] D. J. Wilber, C. Pappone, P. Neuzil, et al. "Comparison of Antiarrhythmic Drug Therapy and Radiofrequency Catheter Ablation in Patients With Paroxysmal Atrial Fibrillation: A Randomized Controlled Trial." In: *JAMA* 303.4 (Jan. 2010), pp. 333–340. ISSN: 0098-7484. DOI: 10.1001/jama.2009.2029. eprint: https://jamanetwork.com/journals/jama/articlepdf/185277/joc90147_333_340.pdf.

[WMC03] W. A. Wattigney, G. A. Mensah, and J. B. Croft. "Increasing trends in hospitalization for atrial fibrillation in the United States, 1985 through 1999: implications for primary prevention." In: *Circulation* 108.6 (2003), pp. 711–716.

[Wu+14] L. Wu, Y. Yao, L. Zheng, et al. "Long-term follow-up of pure linear ablation for persistent atrial fibrillation without circumferential pulmonary vein isolation." In: *Journal of cardiovascular electrophysiology* 25.5 (May 2014), pp. 471–476. ISSN: 1045-3873. DOI: 10.1111/jce.12360.

[Xi+04] Q. Xi, A. V. Sahakian, J. Ng, and S. Swiryn. "Atrial fibrillatory wave characteristics on surface electrogram: ECG to ECG repeatability over twenty-four hours in clinically stable patients." In: *Journal of cardiovascular electrophysiology* 15.8 (Aug. 2004), pp. 911–917. ISSN: 1045-3873. DOI: 10.1046/j.1540-8167.2004.03577.x.

[Yam+15] S. Yamashita, A. Shah, S. Mahida, et al. "Body Surface Mapping to Guide Atrial Fibrillation Ablation." In: *Arrhythmia & Electrophysiology Review* 4 (Dec. 2015), p. 172. DOI: 10.15420/aer.2015.4.3.172.

[Yan+16] Y. Yang, Q. Liu, Z. Wu, et al. "Stiff Left Atrial Syndrome: A Complication Undergoing Radiofrequency Catheter Ablation for Atrial Fibrillation." In: *Journal of cardiovascular electrophysiology* 27 (Feb. 2016). DOI: 10.1111/jce.12966.

[Zhi+16] Z. Zhiwei, K. Letsas, N. Zhang, et al. "Linear Ablation Following Pulmonary Vein Isolation in Patients with Atrial Fibrillation: A Meta-Analysis." In: *Pacing and clinical electrophysiology : PACE* 39 (Mar. 2016). DOI: 10.1111/pace.12841.